

# **Central Lancashire Online Knowledge (CLoK)**

Title	Forced draught impact on Externally Venting Flames: an experimental and
	numerical investigation
Type	Article
URL	https://knowledge.lancashire.ac.uk/id/eprint/57236/
DOI	https://doi.org/10.1002/fam.70019
Date	2025
Citation	Subramania-Warrier, Anoop, Smolka, Jan, Kempna, Kamila, Panchal, Meet, Graham, Tony and Asimakopoulou, Eleni (2025) Forced draught impact on Externally Venting Flames: an experimental and numerical investigation. Fire and Materials. ISSN 0308-0501
Creators	Subramania-Warrier, Anoop, Smolka, Jan, Kempna, Kamila, Panchal, Meet, Graham, Tony and Asimakopoulou, Eleni

It is advisable to refer to the publisher's version if you intend to cite from the work. https://doi.org/10.1002/fam.70019

For information about Research at UCLan please go to <a href="http://www.uclan.ac.uk/research/">http://www.uclan.ac.uk/research/</a>

All outputs in CLoK are protected by Intellectual Property Rights law, including Copyright law. Copyright, IPR and Moral Rights for the works on this site are retained by the individual authors and/or other copyright owners. Terms and conditions for use of this material are defined in the <a href="http://clok.uclan.ac.uk/policies/">http://clok.uclan.ac.uk/policies/</a>





# RESEARCH ARTICLE OPEN ACCESS

# Forced Draught Impact on Externally Venting Flames: An Experimental and Numerical Investigation

Anoop Subramania Warrier<sup>1</sup> 📵 | Jan Smolka<sup>2</sup> | Kamila Kempna<sup>2</sup> | Meet Panchal<sup>3</sup> | Tony Graham<sup>1</sup> | Eleni Asimakopoulou<sup>1</sup> 📵

<sup>1</sup>School of Engineering, University of Central Lancashire, Preston, UK | <sup>2</sup>Faculty of Safety Engineering, VSB-Technical University of Ostrava, Ostrava, Czech Republic | <sup>3</sup>Department of Fire Safety Engineering, The International College of Engineering and Management, Muscat, Oman

Correspondence: Anoop Subramania Warrier (asubramania-warrier@lancashire.ac.uk)

Received: 17 October 2024 | Revised: 5 October 2025 | Accepted: 17 October 2025

Funding: This work was supported by Majaczech, z.s.

Keywords: compartment fires | computational fluid dynamics (CFD) | externally venting flames (EVF) | forced draught conditions | wind-driven fires

#### **ABSTRACT**

Wind can significantly influence fire development and spread in urban and forest environments causing fatal consequences for the public, the first responders, and the environment. Wind-driven fires can have a significant impact on structural fires as wind can increase the fire's intensity, development, and flame spread. Buildings with flammable materials tend to be more vulnerable to wind-driven fires, as suggested by available data and evidence. In this study, medium-scale compartment-façade fire experiments were conducted using a reduced-scale ISO 9705 setup with heptane fuel and varied opening dimensions (20–40 cm) to examine Externally Venting Flames (EVF) under forced draught (FD) conditions. Using thermocouples and bi-directional probes, a systematic analysis of EVF behavior was carried out, providing key insights into flame projection and façade impact. These experimental results were then used to validate computational fluid dynamics (CFD) simulations performed in FDS. A parametric study was conducted to investigate the influence of wind on EVF from fire compartments with different opening dimensions. The research is beneficial in expanding understanding of EVF development using numerical and experimental techniques to study the influence of wind velocity, ventilation conditions and opening dimensions. Predictions of EVF flow, oxygen concentration and temperature profiles were investigated and results indicate that in forced draught conditions there is less thermal impact on façade walls as the wind forces EVF outward and thus increases the EVF projection and decreases its height.

#### 1 | Introduction

Factors such as fuel load, building height, compartment geometry, ventilation, external wind conditions, and compartment opening dimensions play a crucial role in the development and spread of fire and smoke in buildings [1, 2]. In a compartment fire scenario, following ignition, burning gases such as flames or hot unburnt combustion gases may exit through the compartment openings (through doors, windows, etc.) and burn outside when this excess fuel mixes with ambient air; the phenomenon of which is called Externally Venting Flames (EVF) [3]. The rise in such fires has been further exacerbated by modern-day

design preferences and sustainability-focused building practices have prompted the use of diverse façade materials and systems, including those with combustible materials, contributing to an increase in façade fires worldwide [4, 5]. Formation of EVF and associated thermal exposure are primarily associated with the compartment of origin where the fire develops and vents externally and its intensity may be significantly influenced by changes in compartment ventilation, horizontal and vertical openings, and size [1, 6–7]. Significant research has been conducted in the past to study the influence of wind on building fires [8–11] and it is well understood that in many past fire incidents, wind conditions have played a significant role in the

This is an open access article under the terms of the Creative Commons Attribution License, which permits use, distribution and reproduction in any medium, provided the original work is properly cited.

© 2025 The Author(s). Fire and Materials published by John Wiley & Sons Ltd.

**FIGURE 1** | High-rise building fire spread aggravated by wind and combustible cladding [14, 15].

spread of fire and smoke. A few such cases were reported such as the Marina Torch tower in 2015 and 2017 [12]; The Address downtown in 2015 [13], in Dubai, United Arab Emirates. Figure 1 depicts the reported incidents where large fires have resulted from the flame spread over buildings in the neighborhood or community in which wind has been a critical factor, aggravated by the presence of combustible building façade materials [15, 16]. A few of the reported instances of such fires with strong wind that affected the community largely are the Lærdal fire in Norway (2014) [16] and the Cohoe fire in New York (2017) [17].

Understanding the interaction between wind and fire in building façades is critical for improving building fire safety, as this may dictate the behavior of façade fire propagation [17, 18]. International building codes and regulations incorporate a range of passive and active fire safety measures to reduce the likelihood of ignition, limit fire development, and protect life safety, property, and business continuity during building fires. Eurocode 1 (EC1) [19] has provided a design methodology to assess the fire safety of external structural elements based on EVF characteristics, which also considers two ventilation modes, namely No Forced Draught (NoFD) and Forced Draught (FD), with the latter taking the wind factor into account [19]. No Forced Draught (NoFD) condition is when openings are present only on one side of the fire compartment and Forced Draught (FD) conditions are only applicable when there are windows located on opposite sides of the compartment or external influences such as wind or mechanical ventilation systems [19]. When FD conditions apply in cases of openings on two or more walls of the fire compartment it is assumed that flames tend to emerge from one set of openings influencing the rate of heat release, temperature of the fire compartment, flame dimensions (height, horizontal projection, width) and flame temperature emerging from the window [19]. The methodology described in EC1 is limited in nature, due to its prescriptive nature and limitations in accounting for variations in opening size, compartment geometry, and thermal properties; the Eurocode 1 methodology may not be as suitable as performance-based approaches for the fire safety design of complex or unconventional buildings. Studies conducted by Abu-Zidan et al. [20]. suggest that both wind speed and direction have a considerable influence on façade fire propagation. A faster vertical propagation of fire was noticed for the case of no wind but with minimum lateral spread [20]. Further, the research concluded that when the fire is fully developed, the presence of wind can increase the risk of fire spreading along the multiple façade surfaces on the building [20]. Under FD conditions, when the wind is introduced, flames tend to emerge more

forcefully from one dominant opening typically on the leeward or lower-pressure side. This concentrated outflow can increase the horizontal projection of the EVF and lead to reattachment to nearby façade surfaces, particularly in the presence of architectural features such as overhangs, recesses, or balconies. As a result, there is an increased risk of fire spread on multiple external surfaces or adjacent structures, even though the flame originates from a single outlet. Furthermore, as noted by Abu-Zidan et al., wind direction can significantly influence the lateral spread of flames along the building façade [20].

The characteristics of a building, such as its height, shape, and construction materials, have also been found to have a significant impact on the spread and intensity of façade fires. Hu et, al. suggest that compared to a normal compartment fire, the fire behavior of high-rise buildings is more complex due to the special features involved in high-rise buildings, which include complex building structures and larger surface areas with extensive use of external façade insulation materials [21]. Lee et al. conducted a series of small-scale experiments to investigate the influence of a facing wall on externally venting flame behavior. The study examined flame heights, heat fluxes, and general flame dynamics, using a setup in which an opposite parallel wall represented the façade of an adjacent building. This research provides valuable information on the separation distance between the building's external walls, and a new characteristic length scale was developed that gives the length after which the flames turn from horizontal to vertical [22].

EVF from compartment fires are significantly influenced by surrounding boundary conditions, particularly the presence of wind or adjacent structures. It was also observed that when an externally venting flame emerges from an opening facing a nearby wall either opposite or adjacent side wall, the proximity of the surface restricts air entrainment into the plume, resulting in increased flame height and elevated temperatures. This results in higher flame attachment and intensified heat flux to the building envelope [22]. However, in the case of horizontal barriers such as balconies, eaves, etc., this will result in increased air entrainment, and the presence of barriers above will stop the upward momentum of EVF and result in a lesser flame height. However, this can lead to intense heat transfer to the horizontal barrier itself [22].

To investigate the influence of wind, research has been conducted considering different fuel sources including propane gas burners [8, 23–26], heptane pool fires [9, 10, 27–28] or wood cribs

**TABLE 1** | Selected research work on wind-driven medium scale fires.

u (m/s)	Fuel	Comp. dim.  (mm)	Measurements	Variables	No. Vents	References
0-6.0	C <sub>3</sub> H <sub>8</sub>	800×800×800	$T_{\rm in}$ , $T_{\rm out}$ , $u$	u, HRR	2	[8]
0-3.6	$C_3H_8$	$800 \times 800 \times 800$	$T_{\rm in}$ , $u$	u, HRR	2	[8]
0-3.0	$C_7H_{16}$	600×600×600	$T_{\rm in}, T_{\rm out}, u, {\rm HF}$	и	2	[9]
0-3.0	$C_7H_{16}$	$1000 \times 1000 \times 1000$	$T_{\rm in}, T_{\rm out}, u, m_f$	u, pan size	2	[10]
0-2.0	$C_3H_8$	$400 \times 400 \times 400$	$T_{\rm in},T_{\rm out},u,{\rm EVF}_{\rm height}$	u, op. size	1	[25]
0-2.0	$C_3H_8$	$400 \times 400 \times 400$	$T_{\rm in}$ , $T_{\rm out}$ , $u$ , HRR	_	1	[25]
0-2.0	LPG	$400 \times 400 \times 400$	$T_{\rm in}$ , $T_{\rm out}$ , $u$	u, op. size	1	[25]
0-3.5	$C_7H_{16}$	$580 \times 580 \times 580$	$T_{\rm in}, T_{\rm out}, u, {\rm HF}$	<i>u</i> , op. size, fuel posit.	2	[27]
0-3.0	$C_7H_{16}$	$600 \times 600 \times 600$	$T_{\rm in}$ , $T_{\rm out}$ , $u$ , MLR, HRR	и	2	[28]
0-4.4	$C_2H_6O$	$900 \times 900 \times 900$	$T_{\rm in}$ , $T_{\rm out}$ , $u$ , $m_f$	_	2	[31]
0-2.9	C <sub>7</sub> H <sub>16</sub>	900×600×600	$T_{\rm in},T_{\rm out},u,m_f$ EVF	<i>u</i> , op. size	2	Current

[29, 30]. Table 1 shows selected medium-scale experiments from recent literature along with the relevant wind velocity ranges, compartment dimensions, measured quantities (such as temperature at the interior,  $T_{\rm in}$ , exterior,  $T_{\rm out}$ , of the fire compartment, fuel consumption rate,  $m_f$ , heat flux at the façade, HF), parametric studies (such as opening sizes, fuel pan size, and fuel position) and number of openings tested. From those studies, it has been established that increased wind velocity (u) can affect EVF in largely two ways. First, it affects EVF height (EVF<sub>height</sub>) and projection (EVF<sub>proj</sub>), and second, it also affects heat release rate (HRR) and fuel Mass Loss Rate (MLR).

Hu et al. [25]. studied the influence of opening sizes, HRR and u on the EVF and concluded that the EVF height decreases with increasing wind speed. However, it is important to note that this study considered a single opening at the center of the side wall of the fire compartment [25]. Also, Li et al. [8]. studied the wind effect on EVF projection probability from a compartment with opposing opening of different sizes (considers as a door and window) and concluded that when considering the "no wind" case, or wind with very low velocities, there are both inflow and outflow from the openings. However, with increased wind velocities such bidirectional flow will become unidirectional flow at low fuel supply rate and at high wind velocities, only unidirectional flow can be seen at the openings regardless of fuel supply rate [8]. Both studies considered the external wind normal to the opening [8, 25]. However, Hu et al. investigated the influence of wind on EVF where wind is introduced parallel to the façade and concluded that facade flame height decreased with increase in sideward wind speed. Additionally, horizontal flame distance increased for larger opening and decreased for relatively smaller openings with an increase in side ward wind speed [32]. From the existing literature, it can be inferred that the influence of wind, along with its direction, significantly affect the thermal and geometrical characteristics of EVF.

As seen above, previous works have mainly focused on fire compartment and do not fully address how wind affects EVF development and its impact on the façade in varied ventilation conditions with respect to FD and NoFD conditions. The present

study focuses on a reduced-scale compartment with a façade wall on both sides. Openings of equal size are provided at the center of both side walls of the compartment, and an external wind that is normal to the opening was considered. The aim of the present study is to further widen knowledge of EVF development using numerical and experimental techniques to investigate the influence of wind velocity, ventilation conditions and opening dimensions.

#### 2 | Experimental and Numerical Investigation

### 2.1 | Experimental Setup

Figure 2 illustrates the complete experimental setup built, including the smoke extractor's locations, the fire compartment and the two façade rigs at the inlet and outlet. The experimental compartment was built based on a 1:4 scale of the ISO 9705 room, having a length of 900 mm, width of 600 mm, and height of 600 mm and two façade rigs 600 mm width and 600 mm height installed at the inlet and outlet side. It was constructed of 50 mm thick fire-resistant vermiculite boards (THERMAX ECO) and facade rigs were made of fiber cement boards. Both openings on inlet and outlet side were placed under hoods for smoke extraction with dimensions of 1000 mm × 1000 mm. The smoke extractor was connected to an industrial centrifugal blower extractor fan with a capacity of 2600 m³/h.

For the parametric study, it was decided that three sizes of opening dimensions, such as  $200\,\mathrm{mm} \times 200\,\mathrm{mm}$ ,  $300\,\mathrm{mm} \times 300\,\mathrm{mm}$ , and  $400\,\mathrm{mm} \times 400\,\mathrm{mm}$ , which are located on opposite sides, would be investigated. An external wind speed of  $2.9\,\mathrm{m/s}$  was set normal at a distance of  $2.5\,\mathrm{m}$  from the opening to simulate FD conditions for all three opening sizes. The fan was set to start when the fire was fully evolved in the compartment, e.g., when the compartment temperature reaches  $500^{\circ}\mathrm{C}$  or when EVF are visible; whichever happens first, as this will ensure to investigate the characteristics and consequences of EVF on the façade extensively. Current work builds up on the previous experimental work of the authors on forced draught conditions

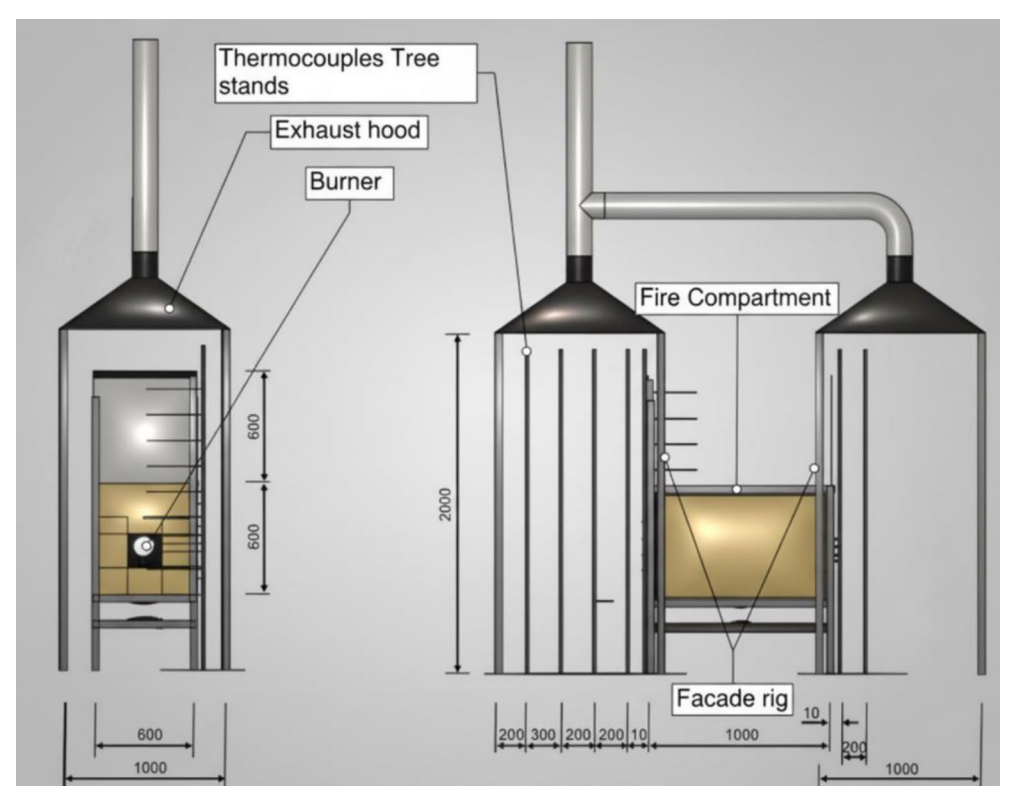


FIGURE 2 | Front and side view of the experimental setup (dimensions in mm).

in enclosure fire development [33]. In these previous experiments, an extensive range of different fan speeds, from 0 m/s (no wind) to 3.5 m/s at different horizontal fan distances from the opening (ranging from 1.5 to 4.5 m), were studied and critical conditions relevant to the study (with respect to the mass loss rate, heat release rate, temperature, uni- and bi-directional flow) were observed at a fan speeds of 2.6–2.9 m/s [33]. In each experiment, 500 g n-heptane was used as the fire source, placed in a  $200\,\mathrm{mm} \times 200\,\mathrm{mm}$  steel pan made of  $2\,\mathrm{mm}$  steel sheets and welded at the center of the compartment.

The medium-scale compartment-façade fire test was designed to investigate the feasibility of simulating full-scale physical phenomena in a reduced-scale experiment by preserving key nondimensional parameters. The Buckingham Pi theorem has been applied to scale down the fire power to be used in the medium scale experimental configuration, ensuring the preservation of the second group ( $\Pi$ 2) as specified in Equation (1) [34]. The  $\Pi$ 2 group is derived from the energy conservation equation, it requires that the model fire power is selected in conformity with the prototype as specified in Equation (2). The length scales  $l_p$  and  $l_m$  correspond to the physical dimension of the prototype and model system respectively, with their ratio  $\frac{l_m}{l}$  being  $\frac{1}{4}$ . The fire power measured during the test conducted in the compartment varied between 250 and 350 kW. Here,  $\dot{Q}$  denotes the heat release rate (HRR), while  $Q_m^*$  and  $Q_p^*$  represent the HRR, in kW for the model and the proto type respectively. The terms  $\rho_{\infty}, C_{p,} \top_{\infty}$  and g are the density in kg/m³, specific heat in kJ/kg K, temperature in Kelvin under ambient conditions and g is the gravitational acceleration in m/s<sup>2</sup>.

$$\Pi_2 = \frac{\dot{Q}}{\rho_\infty C_p \mathsf{T}_\infty \sqrt{g(l)^{5/2}}} \tag{1}$$

**TABLE 2** | Main parameters of the test setup and the corresponding full-scale experiment.

Main parameters of test setup	Reduced scale	Full scale
Compartment length/width/height (mm)	900/600/600	3600/2400/2400
Opening width/ height (mm)	200/300/400	800/1200/1600
Fire Power (kW)	250/350	8000/11200

$$\frac{{Q_m}^*}{{\rho_\infty C_p}{\top_\infty \sqrt{g}{(l_m)}^{5/2}}} = \frac{{Q_p}^*}{{\rho_\infty C_p}{\top_\infty \sqrt{g}{(l_p)}^{5/2}}} \Rightarrow {Q_m}^* = {Q_p}^* \left(\frac{l_m}{l_p}\right)^{5/2} \endaligned$$

In Table 2, the geometrical dimensions of the reduced scale setup and the corresponding full-scale compartment are shown.

To measure the mass loss rate, which was further used for calculating HRR, a scale made from an Arduino, a 20 kg load cell sensor, and 24 bit Analog/Digital convertor HX711 were used. The scale was constructed from 3D-printed parts made of PET-G with adequate robustness and durability and calibrated with accuracy of 1 g. STL files are published on Thingiverse [35]. A total of 72 K-type thermocouples with a bead diameter of 1.5 mm were used for measurement of the temperature profile of compartment fire and EVF. In this work, thermocouples with the limits of error values of  $\pm 1.1^{\circ}$ C or  $\pm 0.4\%$  have been used [36].

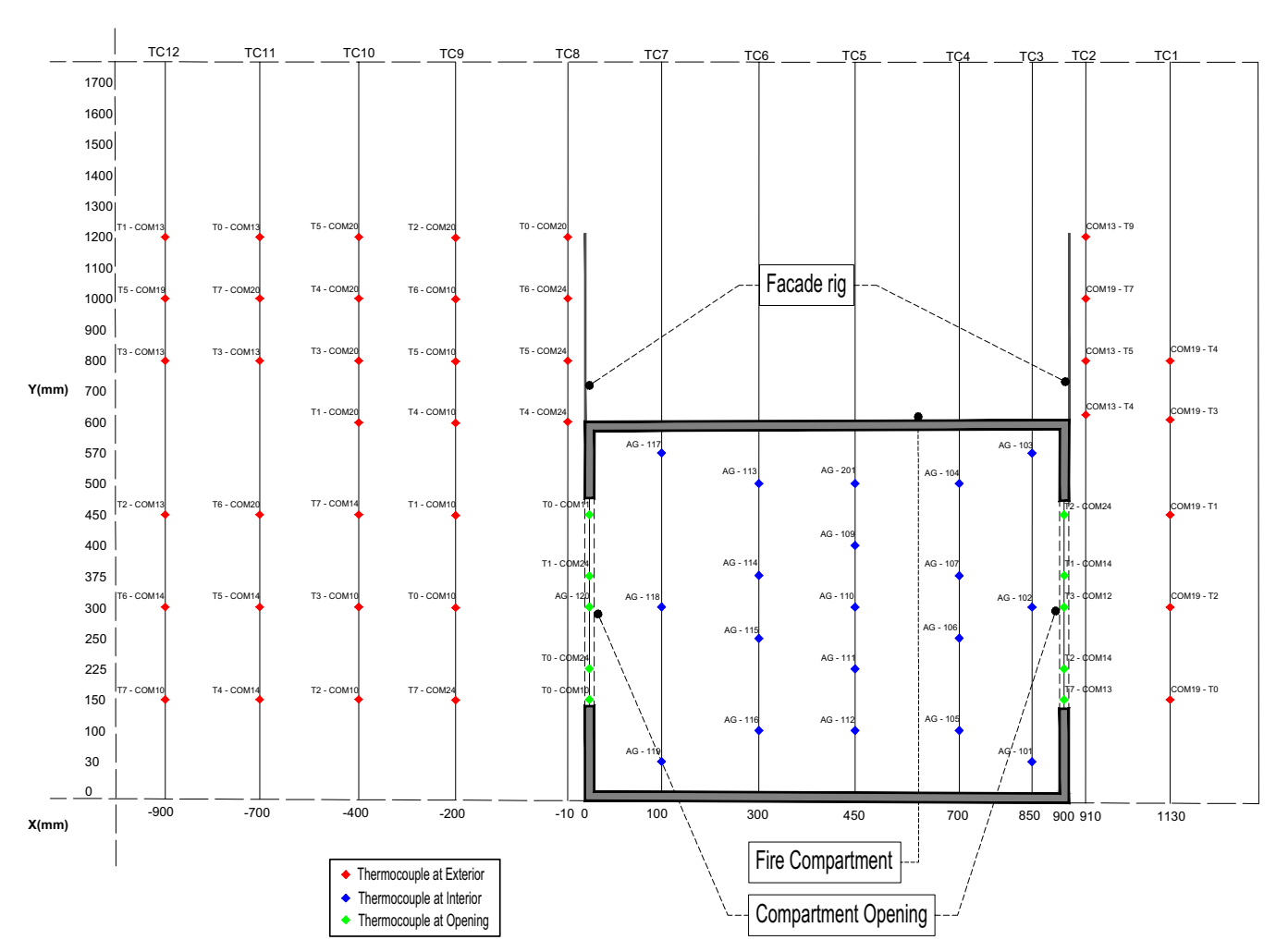


FIGURE 3 | Thermocouples layout at the experimental configuration.

The schematic of measuring instruments is shown on Figure 3 which describes the locations of thermocouples located in the internal and external spaces of the experimental setup on 12 thermocouple trees. Thermocouples were positioned horizontally extending outward from the side of the façade wall, to capture the gas temperature distribution adjacent to the façade. Because EVF may induce high fire plume velocities, which could cause displacement of thermocouples, one of the main design requirements for the measurement system was to ensure that the spatial position of the thermocouple tips remained unaltered during the tests. Prior to each fire test, the thermocouples were carefully positioned and aligned, and post-test inspection confirmed that the majority of the thermocouple tips remained in their intended positions.

The airflow velocity and hot gas pressure difference inside the compartment were measured using a bi-directional velocity probe (BDVP). The probe was calibrated in a custom 3D-printed wind tunnel, as described and validated by Smolka et al. [37] and consistent with the original calibration methodology of McCaffrey & Heskestad [38]. This setup enables velocity measurements up to  $4\,\mathrm{m/s}$  with a standard deviation of 1.2% and a turbulence intensity of 1% [37]. Prior to each fire test, the airflow field generated by the fan was evaluated in the absence of combustion to ensure stability and uniformity. The results showed a relatively consistent velocity profile, with variations within  $\pm 5\%$ 

across the measurement grid—demonstrating that the flow field was reasonably uniform in the region of interest [37]. The fan used in the experiments was positioned 2.5 m from the compartment opening, with the intention of creating a uniform forced draught condition at the plane of the compartment opening. The air velocity of 2.9 m/s refers to the average velocity measured at the center of the compartment opening during pre-fire testing using a calibrated BDVP [37]. The fan outlet itself had a circular cross-section with a diameter of 350 mm, and the airflow profile was reasonably uniform across the horizontal centerline of the opening due to the fan distance and axial alignment. The BDVP and thermocouple locations are described in the openings shown in Figure 4.

Table 3 describes the list of experiments, including wind speed, opening dimensions, and ventilation factors used for the experiments.

## 2.2 | Numerical Setup

To investigate the influence of FD conditions on the development of an EVF, the experimental test cases mentioned in Table 2 have been simulated using the Fire Dynamic Simulator (FDS, Version 6.7.9) [39]. Developed by NIST, the FDS code is a CFD tool designed to address fire protection engineering problems by investigating

Fire and Materials, 2025 5

fundamental fire dynamics and combustion. The simulation solves a form of the Navier–Stokes equations, which are suited for low-speed, thermally driven flows and focus on smoke production and heat transfer from fires, using a 3D Cartesian grid [39]. The numerical model was designed to replicate the experimental configuration and dimensions. All solid surfaces, including walls and floors, are

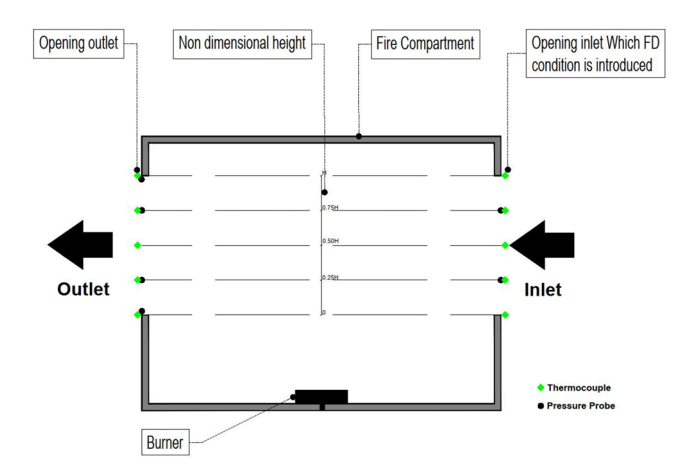


FIGURE 4 | Thermocouples and BDVP location at the openings.

**TABLE 3** | Experimental test scenarios.

	Opening dimensions			Wind
Test cases	Width (m)	Height (m)	Ventilation factor (m <sup>5/2</sup> )	speed (m/s)
NoFD- 20×20	0.20	0.20	0.0358	0.0
FD- 20×20	0.20	0.20		2.9
NoFD- 30×30	0.30	0.30	0.0986	0.0
FD- 30×30	0.30	0.30		2.9
NoFD- 40×40	0.40	0.40	0.2024	0.0
FD- 40×40	0.40	0.40		2.9

provided with boundary conditions with the material properties corresponding to the experimental setup. Figure 5 shows the experimental along with the numerical setup. The soot yield, which represents the fraction of heptane fuel mass converted to smoke particulates, was set equal to  $0.015\,\mathrm{kg/kg}$  and the corresponding CO yield was set equal to  $0.006\,\mathrm{kg/kg}$  [40]. FDS incorporates a submodel for wind that imposes mean flow velocities based on Monin-Obukhov similarity parameters. This method enables the modeling of velocity and temperature profiles as a function of height within the domain, taking into account aerodynamic roughness length, scaling potential temperature, and the Obukhov length [39, 41]. However, the experimental setup in the current study uses a fan to establish the FD conditions, which is represented in FDS by modeling a vent with a constant velocity profile of  $2.9\,\mathrm{m/s}$ .

#### 2.2.1 | Computational Domain

The computational domain was selected to accurately represent the flow and thermal characteristics of the EVF flame. However, an increased domain was chosen for the FD condition in all cases, as the fan was placed at a distance of 2.5 m from the edge of the opening. The domain was extended 1 m in the positive and negative X axes for the NoFD conditions from the edge of the respective openings on the opposite side of the compartment and 2.7 m in the positive X axis for the FD due to the location of the fan. The increased domain dimensions considered are depicted in Figure 6 below.

#### 2.2.2 | Grid Independence

The non-dimensional expression  $D^*/dx$  is a measure of how well the flow field is resolved in the simulation of buoyant plumes, where dx is the size of cells and  $D^*$  is the characteristic fire diameter [39]. The  $D^*/dx$  ratio indicates the adequacy of the grid resolution. A higher  $D^*/dx$  would mean a better resolution for the simulation of fire, as FDS uses a structured mesh. A grid sensitivity analysis for three different D\*/dx values namely 4 (coarse mesh), 10 (moderate mesh), 16 (fine mesh) was conducted and results for the temporal evolution of temperature and velocity at the middle of the opening for the case of FD-20×20 of FD condition are depicted in Figure 4. The D\*/dx ratio of 16 was found to be optimal in terms of accuracy with a corresponding cell size of 0.02 m. Further to this, to reduce the computational time for the simulation, an additional sensitivity analysis was performed with multiple mesh sizes. To capture the buoyant plume and fire flow field accurately, the inside of the compartment is provided

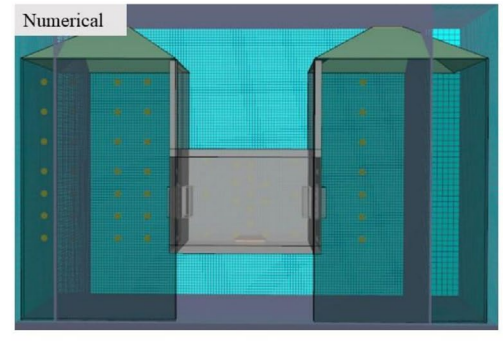




FIGURE 5 | Numerical (left) and experimental (right) setup.

with a 0.02 m mesh and the rest (both sides of the opening) with a 0.04m mesh size. However, a coarse mesh was deemed insufficient for the test cases as it failed to accurately resolve the flow field for fire simulation; thus it was not included in the study. Additionally, the fine mesh was tested using two approaches: a single uniform mesh and a multi-mesh setup with the same cell size. Figure 7 plots temperature and velocity values at the opening's center, showing that moderate mesh results are slightly higher with more fluctuations compared to the others. The results from both fine mesh approaches showed no significant differences in terms of velocity and temperature. The multiple mesh configuration with 0.02 m cell size was adopted for numerical simulations, as it provided the same level of accuracy while significantly reducing computational time. The total computational grid consisted of 498432 cubic cells for NoFD conditions and 542784 cubic cells for FD conditions.

#### 2.2.3 | Turbulence Model

A preliminary study of turbulence models including Large Eddy Simulations (LES), Very Large Eddy Simulations (VLES), and Simply Very Large Eddy Simulations (SVLES) was conducted for the case FD-20×20 to ensure proper modeling of flow turbulence. Figure 8 plots the resulting temperature and velocity at the opening's center, indicating that SVLES has a wider range with more fluctuations compared to LES and VLES. However, the current study uses Large Eddy Simulations (LES) to model flow turbulence with the Smagorinsky sub-grid scale model [42]. The Smagorinsky model's constant value,  $C_s$  = 0.2, and the CFL region of 0.8 and 1, along with a *Schmidt* and *Prandtl number* of 0.5 were used. Previous studies [43] have shown that the Smagorinsky model performs well in simulating wind flow.

#### 2.2.4 | Validation of Numerical Simulation

To validate the numerical results, experimental data of FD  $20\times20$  case was used to analyze the temporal evolution of velocity and temperature measurements at the opening's center. The validation of these velocity and temperature measurements is considered important to determine outward gas temperature and its velocity for the FDS validation. Figure 9 thus illustrates

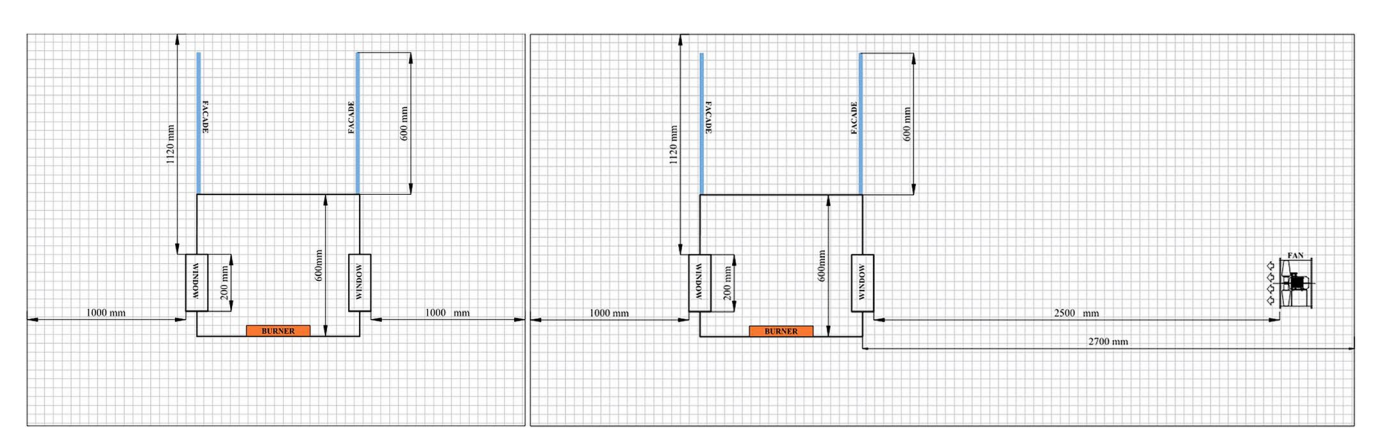


FIGURE 6 | Computational domain and relevant dimensions of the model NoFD (left) and FD (right).

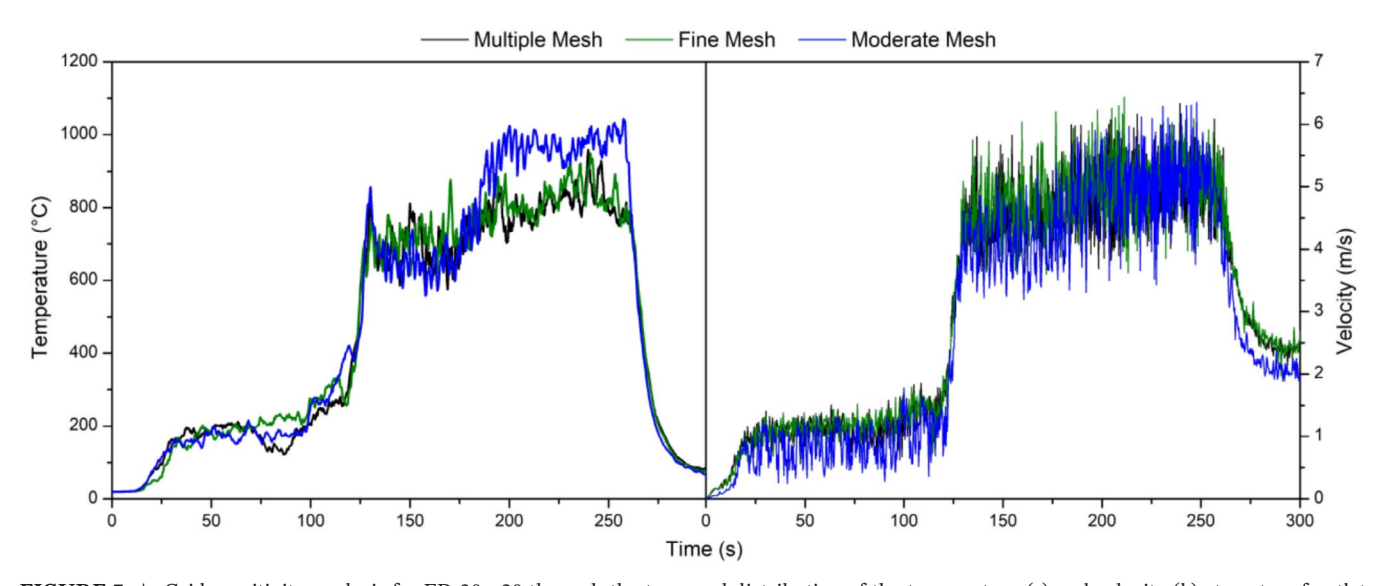


FIGURE 7 | Grid sensitivity analysis for FD-20×20 through the temporal distribution of the temperature (a) and velocity (b) at center of outlet opening.

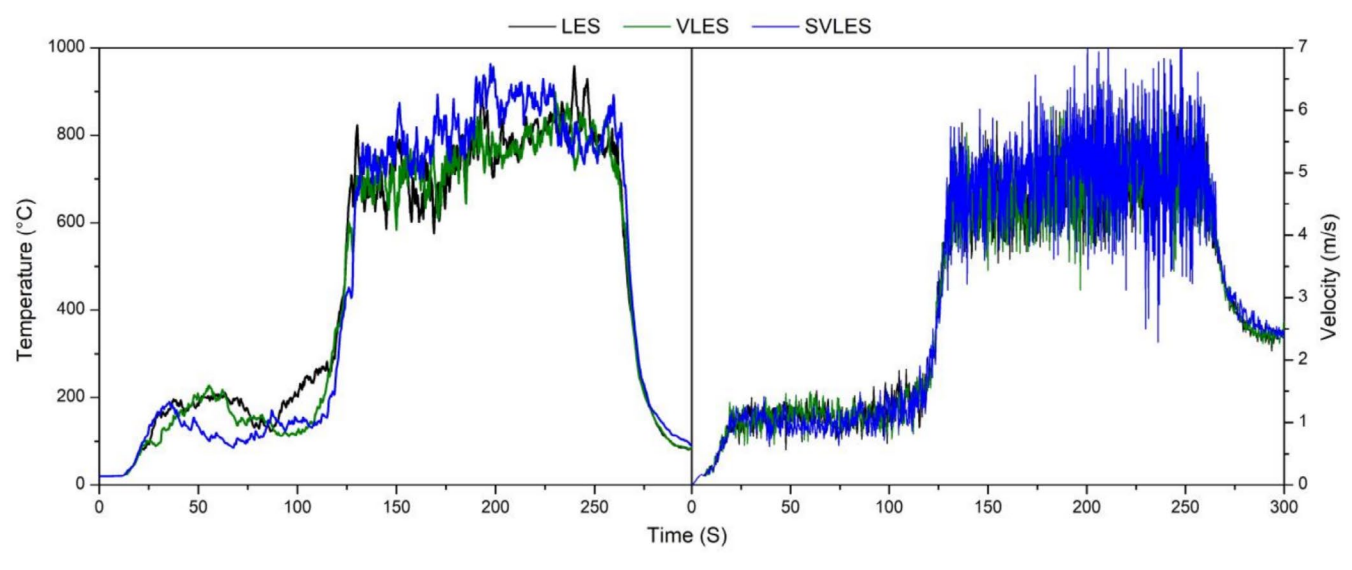
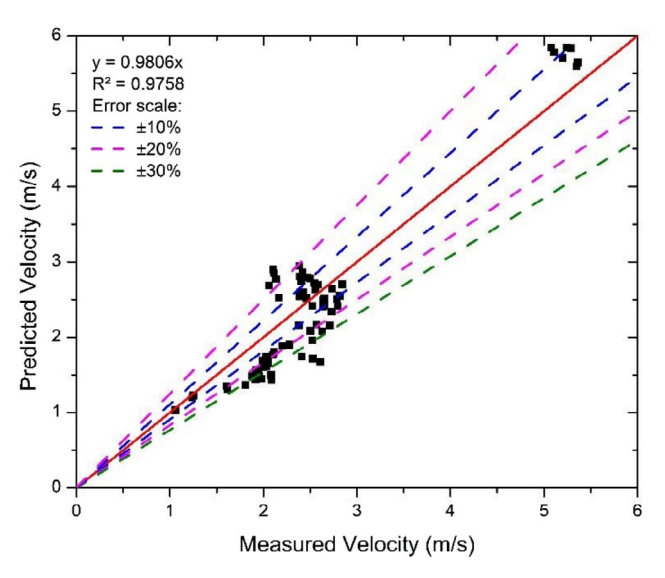
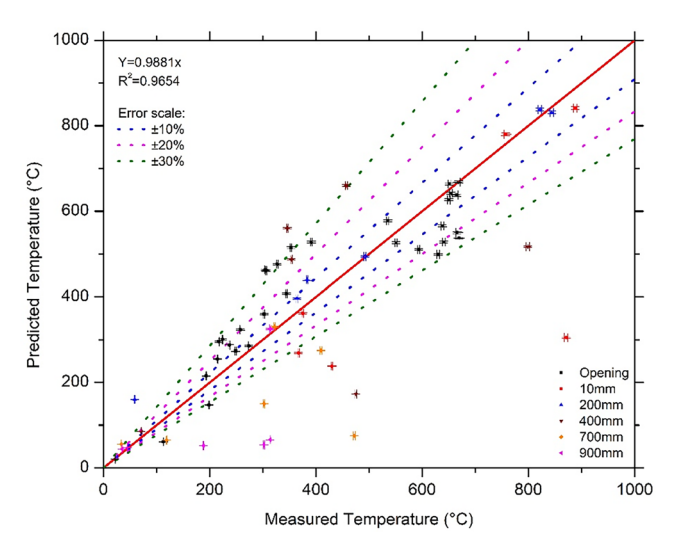


FIGURE 8 | Temporal distribution for FD-20×20 of the temperature (a) and velocity (b) at center of the outlet opening for different LES models.



**FIGURE 9** | Validation based on predicted velocity at center of outlet opening for NoFD 20×20.

the outward gas velocity for the FD 20×20 case, where the vertical axis represents numerical results and the horizontal axis represents experimental data. The error margins are represented by dotted lines, and the red diagonal dashed line indicates a perfect match between simulation and experimental data. Figure 9 presents the temporal velocity values obtained from both the experimental measurements and the numerical simulation at the center of the outlet opening. In the numerical results, the velocity is represented as a single scalar value corresponding to the magnitude of the total velocity vector, computed from the three orthogonal components. These values were directly compared with experimental data recorded using a Bi-Directional Velocity Probe (BDVP). The data show that 70% of the predictions fall within a  $\pm 30\%$  error margin, indicating good agreement. The  $R^2$ value, also known as the coefficient of determination, is found to be 0.9, and the linear regression slope is approximately 1, suggesting a moderate-to-strong positive linear relationship and a good fit for the data.



**FIGURE 10** | Validation based on predicted temperature at center of outlet and temperature distribution at horizontal distances of 10–900 mm.

Figure 10 depicts the validation case for temperature at the center of the opening. The validation also considered the temperature distribution at horizontal distances of 10-900 mm. The data in Figure 10 presents temporal temperature measurements obtained from both experimental observations and numerical simulations at the center of the outlet opening. In addition, temperatures measured by the thermocouple tree, positioned at horizontal distances of 10-900 mm with sensors located at different heights (as shown in Figure 3), were analyzed using a 20-s time-averaging window applied over the period from 310 to 330s after ignition. This interval corresponds to the fully developed fire stage, during which flame behavior was stable and externally venting flames were consistently observed. For the current validation case, the focus is primarily on the outward-flowing gas temperature distribution. Additionally, the model considered the temperature distribution at the opening and façade for different opening sizes and compared these results with experimental results in sections 3.1 and 3.2, respectively. The data show that 70% of the predictions fall within

a  $\pm 30\%$  error margin, indicating good agreement. The  $R^2$  value is found to be 0.98, and the linear regression slope is approximately 1, suggesting a moderate-to-strong positive linear relationship and a good fit for the data.

#### 3 | Result and Discussion

# 3.1 | Effect of Opening Size on EVF Thermal Characteristics

Figure 4 depicts the placement of five thermocouples at equal intervals at the compartment openings for the various opening sizes. Figure 11 presents the temperature readings from five thermocouples positioned at varying heights along the compartment opening for the NoFD 20×20 experimental setup. For the NoFD cases, the experimental setup was fully symmetric, with identical opening dimensions and boundary conditions on both sides of the compartment. During testing, the EVF behavior and temperature measurements at both openings were observed to be consistent, to avoid redundancy and maintain clarity, Figure 11 presents the temperature results from one representative opening. It was observed that the flame consistently spilled out of the opening around 310s, coinciding with the time when the fuel was nearly fully consumed. Data collection ceased at approximately 350s. The recorded data from the loggers were analyzed, and the selected data represents the time-averaged values for a 20-s period, spanning from 310 to 330 s, when the fire was at its peak and flames were visible outside. This approach was applied consistently across all experiments, where data were analysed, and the selected data represents the time-averaged values for a 20-s period. To assess the sensitivity of the 20-s averaging window, we performed an additional analysis using 10-s, 15-s, and 30-s time-averaging intervals centred around the fully developed fire period (310-330s). The variation in the average temperature values was found to be within ±5% for the 10and 15-s windows. However, the 30-s average showed up to  $\pm 10\%$ variation, as in some cases this interval fire extended into the decay phase where the mass burning rate dropped significantly. For consistency and reliability, we used the mean value over the 20-s interval in all comparisons, rather than the midpoint value. This

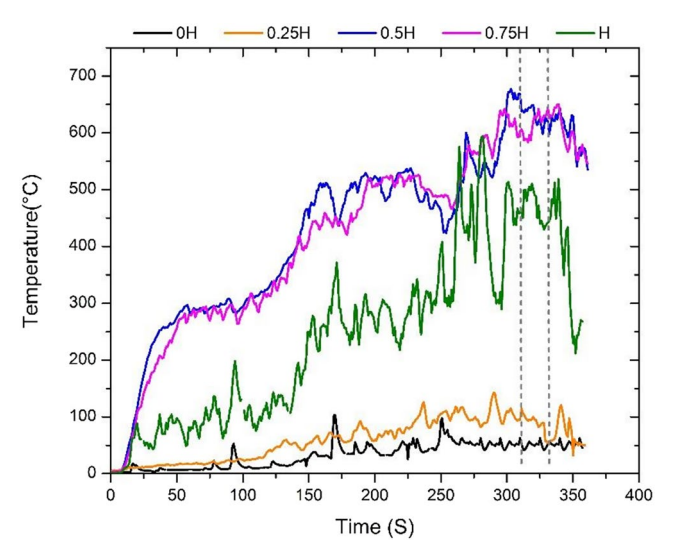


**FIGURE 11** | Temperature measurement at the opening for the case of NoFD  $20 \times 20$ .

method ensured that transient fluctuations were smoothed out while still capturing the peak fire behavior in a stable phase. Also, to ensure consistency across all test cases, a 20-s time-averaging window (where flame consistently spilled out from the opening) was applied to thermocouple measurements, chosen to reflect the steady-state EVF condition, regardless of the exact burn duration.

Figure 12 depicts the experimental and numerical analysis (FDS) results for all the three different wall opening sizes, under NoFD and FD conditions. The term "non-dimensional height" refers to the relative placement of thermocouples along the opening height (H) of the compartment. For each opening size (20, 30, and 40 cm), thermocouples were placed at five discrete vertical positions: 0H, 0.25H, 0.5H, 0.75H, and H, where H corresponds to the full opening height. This approach enables consistent comparison of temperature distributions across different opening configurations by normalizing sensor locations relative to opening height.

For experiments under NoFD conditions, it can be observed that there is a decrease in temperature in the middle of both the wall openings with the increase in wall opening dimensions. Also, temperature values at the top of the compartment opening increase with the increase in the compartment opening dimension. This is mainly due to the change in the opening size, which influences the air entrainment and the exiting of EVF gases. For wall opening sizes 20 and 30 cm, (NoFD-20×20 and NoFD-30×30 cases) the FDS and experimental results are in good agreement. However, for the 40 cm wall opening (NoFD-40×40 case), there is a major difference in the FDS and experimental results, for the temperature at the bottom of the compartment opening. This is due to the evident bi-directional flow in and out of the compartment, with more fresh air entering the compartment from the lower part of the opening during the FDS simulation. Additionally, FDS uses a simplified chemistry approach for turbulent combustion. In FDS, the experimentally measured MLR was prescribed directly as an input parameter. While this approach ensures that the target MLR is accurately modeled, it also means that the combustion model accuracy is not adequately predicting experimentally measured MLR in under-ventilated conditions. This behavior is consistent with the limitations of the simplified combustion treatment in FDS: although it reproduces the experimentally measured MLR, it does not fully resolve the fire and ventilation dynamics. Consequently, in the 40×40 opening case, this limitation can accentuate discrepancies between numerical predictions and experimental measurements For the no-wind condition for all three opening sizes, bidirectional flow was observed, whereas in the FD condition only unidirectional flow was observed in the experiment.

During the experiments under FD conditions, temperature profiles at compartment openings are higher compared to the NoFD conditions. It is noted that as the compartment opening dimension increases, the temperature in the center of the compartment opening decreases. For compartment openings 20 and 30 cm (FD- $20\times20$  and FD- $30\times30$  cases), it is noted that the temperatures are almost identical, except the value for the thermocouple at the bottom. In contrast to NoFD conditions, it is observed that once the fire is fully evolved with forced draught, there is only unidirectional flow through the compartment opening instead of bidirectional flow. In the 20 and 30 cm FDS cases, it is observed that a uniform temperature profile is maintained through the entire opening. For 40 cm openings, flames are exiting mainly through

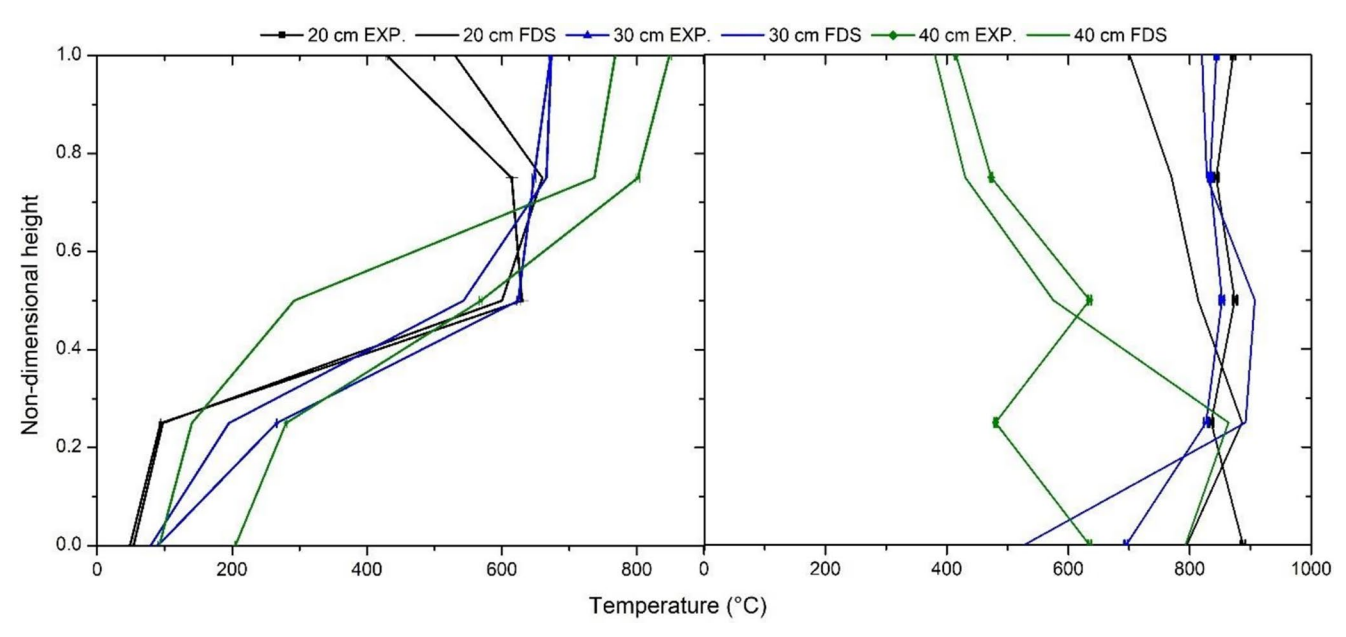


FIGURE 12 | Non dimensional vertical distribution of the temperature at the outlet opening for NoFD (left) and FD (right) conditions.

the lower part of the opening, and thus there is an increased temperature in the lower part of the opening. This can be attributed to the fact that with forced draught wind resulting in more efficient airflow exchange. This further results in increased burning within the fire compartment pushing the flames outwards, also changing the fire dynamics within the fire compartment. For cases with 40 cm openings and FD conditions more flames will exit through the bottom of the opening as there is a larger opening dimension. This behavior was observed specifically in the FD 40×40 case, where the forced draught induced by the fan significantly influenced the flow field at the compartment opening. Due to the increased vertical height of the opening, the incoming airflow from the fan primarily goes through the upper portion, while the hot gases and flame are pushed downward, exiting through the lower part of the opening. The wind effect causes the flame to tilt downward. In contrast, for cases with smaller opening heights (e.g., 20 and 30 cm), the entire opening is generally filled with flame. Additionally, a notable discrepancy in temperature was observed at the lower part of the opening in the FD-40×40 case when comparing experimental and simulation results. This variation is primarily attributed to the turbulence model employed in the numerical analysis. As the opening size increases and wind influence is introduced, turbulence becomes more pronounced, leading to greater modelling uncertainty. In addition, the influence of radiative heat flux on thermocouple readings can lead to higher measured temperatures in experiments. Although the FDS thermocouple model accounts for this effect to some extent, since the thermocouple (TC) model, temperature lags the true gas temperature depending mainly on bead size. During the experiments, sheathed thermocouples were used to mitigate direct radiative effects. The presence of multiple metal and air gaps in the thermocouple device construction may limit the model's ability to fully capture the complex radiative-convective balance. This limitation is particularly relevant for scenarios with strong flame impingement, such as the  $40 \times 40$  opening case.

To investigate the EVF temperature profile outside the compartment opening, a further analysis has been carried out

considering horizontal distances of 10, 200, 400, 700, and 900 mm, normal to the compartment opening center, and results are plotted in Figure 13. A total of 35 thermocouples were positioned as depicted in Figure 3 to effect a temperature analysis of the EVF spilling out from the opening. However, only the data from the thermocouples that are located normal to the compartment opening center line were considered for the analysis. The selected data is the time average for a period of 20 s, when the fire is at its peak for all the experiments.

It was observed that the temperature at the centerline of the opening decreases with the increase in horizontal distance, in NoFD conditions, for all opening sizes. Furthermore, as the vertical distance from the opening increases, the EVF temperature is observed to be increasing as well. This agrees with results agreed with Asimakopoulou's [5] that presented time-averaged temperature contours at the centerline plane perpendicular to the façade of medium-scale experiments demonstrating that the developing EVF temperatures gradually decrease with increasing height and projection from the façade. The EVF shape has been demonstrated to depend on both the fire load and the opening geometry resulting in the total volume of the EVF envelope increasing with increasing fire load and opening area.

Maximum temperature was measured at a distance of 10 mm in NoFD condition and in FD, the maximum temperature appears at 200 mm. The overall horizontal temperature profile for the FD conditions is much higher in consideration to the NoFD conditions. For the 20 and 30 cm cases, similar temperature profiles were identified; however, in the 40 cm case, less overall temperatures were observed. The numerical results exhibit good agreement with the experimental results. Under the NoFD conditions, there is an average percentage of approximately 6% in values when compared to the outcomes of the numerical analysis. Similarly, in the FD conditions, there is an approximately 15% temperature differential, as shown in the Figure 13.

### 3.2 | Effect of Opening Size on the Façade

Thermocouples were positioned in the façade as depicted in Figure 3. Figure 14 shows the temperature profile at the façade for NoFD and FD conditions. The temperature for the 40 cm compartment opening (both FD-40×40 and NoFD-40×40) during numerical and experimental analysis in NoFD, is not in agreement. This is due to the turbulence modeling issue with numerical analysis. A similar observation is found in the 30 cm FD-30×30 case with FD conditions. In NoFD conditions, the 30 and 40 cm opening sizes (NoFD-30×30 and NoFD-40×40) were showing increased temperatures when compared to the 20 cm opening size (NoFD-20×20). In FD conditions, for all opening sizes, the façade temperatures were observed to be less, when compared to the NoFD condition. This is due to the forced draught wind pushing the EVF gases outwards, and thus increasing the horizontal projection and there is a

corresponding decrease in the flame height. The decreased flame height leads to a diminished radiative and convective thermal impact on the façade surfaces in FD conditions relative to NoFD conditions. This finding is consistent with the results reported by Ren et al. [44]. who conducted small-scale compartment fire tests in a wind tunnel. Ren's study found that the maximum temperatures measured on the façade decreased with increasing wind velocity from 0 to 2.0 m/s. In NoFD conditions, an average temperature increase exceeding 30% was observed for the 20 cm case, while the temperature increased by 150% and 200% for the 30 and 40 cm NoFD cases, respectively. Numerical results of façade temperatures under NoFD conditions for the 20 and 40 cm cases, are in good agreement with experimental results as there is an average percentage of approximately 7%, but this was increased to 10% when compared with experimental measurements of temperature under FD conditions.

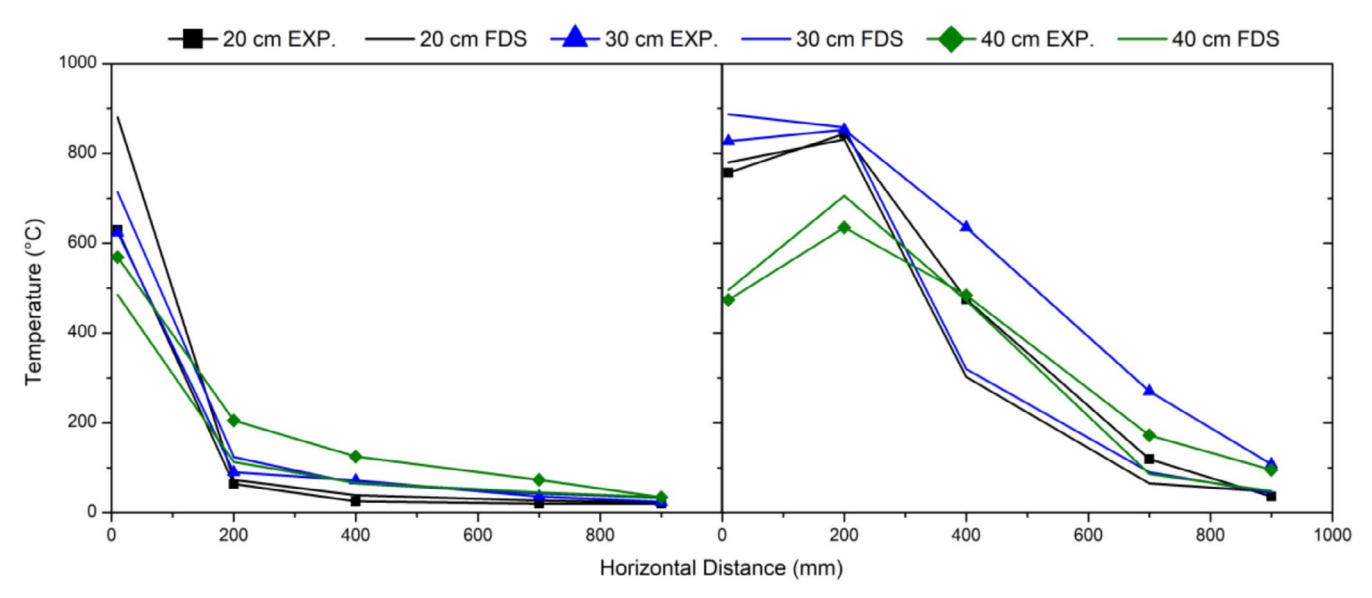


FIGURE 13 | Temperature profile versus the horizontal distance at the center of the outlet opening for NoFD (left) and FD (right) conditions.

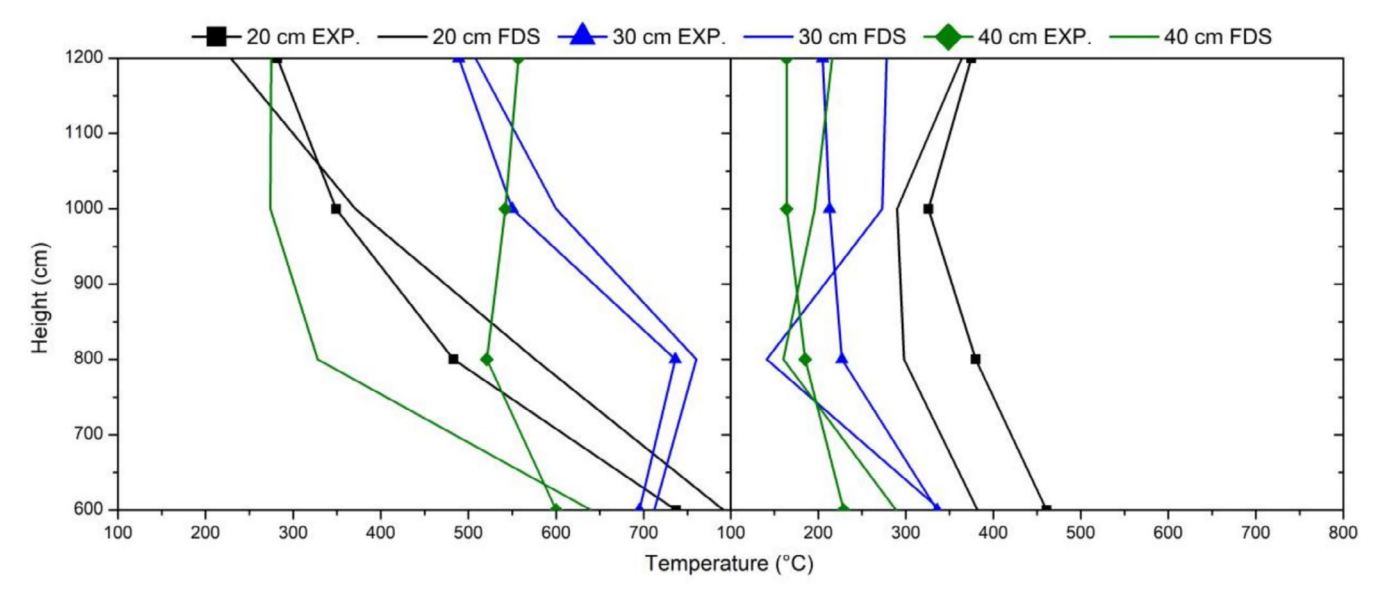


FIGURE 14 | Vertical distribution of the temperature profile at the centerline of the outlet façade for NoFD (left) and FD (right) conditions.

### 3.3 | Developed Thermal Field

The evolution of the thermal field near the façade was analysed under both NoFD (no forced draught) and FD (forced draught) conditions for two different façade geometries (20 and 40 cm), as presented in Figure 13. The analysis focuses on representative time points that capture the fully developed fire stage, during which external flames were consistently visible and the wind flow, when applied, had reached a steady state. Instead of time-averaged 20 s slice files in Smokeview, instantaneous snapshots were chosen to present the thermal field. This is because the overall profiles and values obtained from the averaged slice files are comparable to those from the instantaneous snapshots presented in Figures 15 and 16. The primary difference is that the averaged plots exhibit smoother contours with reduced turbulence, which is consistent with the expected effect of temporal averaging.

For the 20 cm façade geometry, temperature distributions are shown at 150 s. This time point was selected as it corresponds to the period when the fire had fully evolved, the fan was operating in the FD scenario, and the wind flow had stabilized. Similarly, for the 40 cm façade geometry, results are presented at 200 s, which also marks the fully developed fire stage with established external flaming and a steady wind field. These selections ensure comparability between cases in terms of fire development and ventilation state.

The thermal field shows significant differences between NoFD and FD conditions. Under FD conditions, temperatures near the compartment opening reached values between 700°C and 800°C. However, as the external plume rose, a rapid

temperature decay was observed due to increased air entrainment and mixing. Inside the compartment, the forced ventilation disrupted thermal stratification, resulting in relatively uniform and much lower gas temperatures ranging from approximately 30°C–100°C. This mixing effect is characteristic of wind-driven ventilation and limits the build-up of hot gas layers.

In contrast, NoFD conditions led to the formation of distinct thermal stratification within the compartment. Higher gas temperatures, in the range of 700°C–900°C, were observed in the upper layer near the opening. The absence of wind allowed for a more vertically extended flame, which increased the thermal impact on the façade surface. These differences in flame behaviour under varying ventilation conditions are clearly reflected in the façade temperature distributions.

For the 40cm façade, NoFD conditions resulted in maximum temperatures along the façade surface between 600°C and 750°C, indicating strong exposure. In comparison, the 20cm façade under NoFD conditions exhibited lower façade surface temperatures, around 150°C–200°C, suggesting a more confined heat plume and reduced external exposure. Under FD conditions, both façade geometries experienced significantly reduced temperatures at the façade surface, highlighting the dampening effect of wind on vertical flame spread.

The results clearly indicate that forced draught plays a critical role in modifying fire plume behaviour and reducing thermal exposure to external surfaces. The presence of wind suppresses plume rise, limits external flame height, and promotes mixing, which collectively result in lower façade temperatures. These

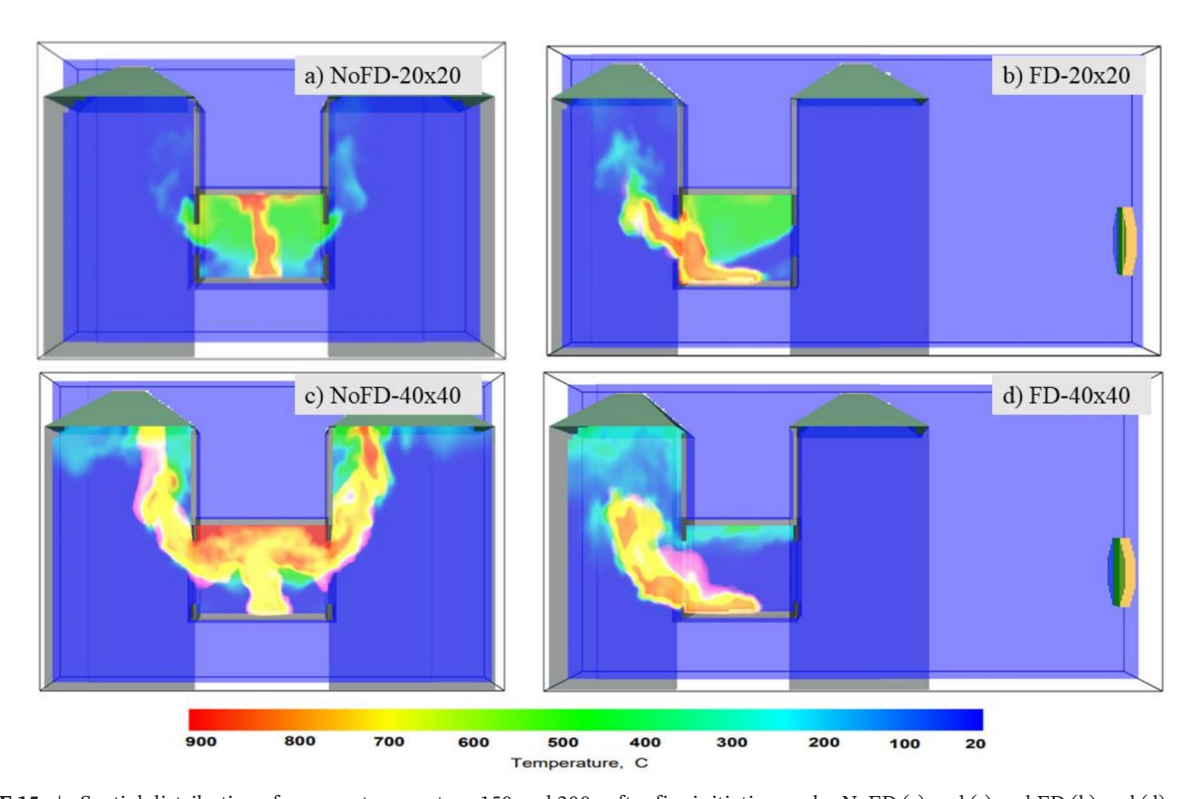


FIGURE 15 | Spatial distribution of gaseous temperature 150 and 200s after fire initiation under NoFD (a) and (c) and FD (b) and (d) conditions; 20 cm (top) and 40 cm (bottom) opening size.

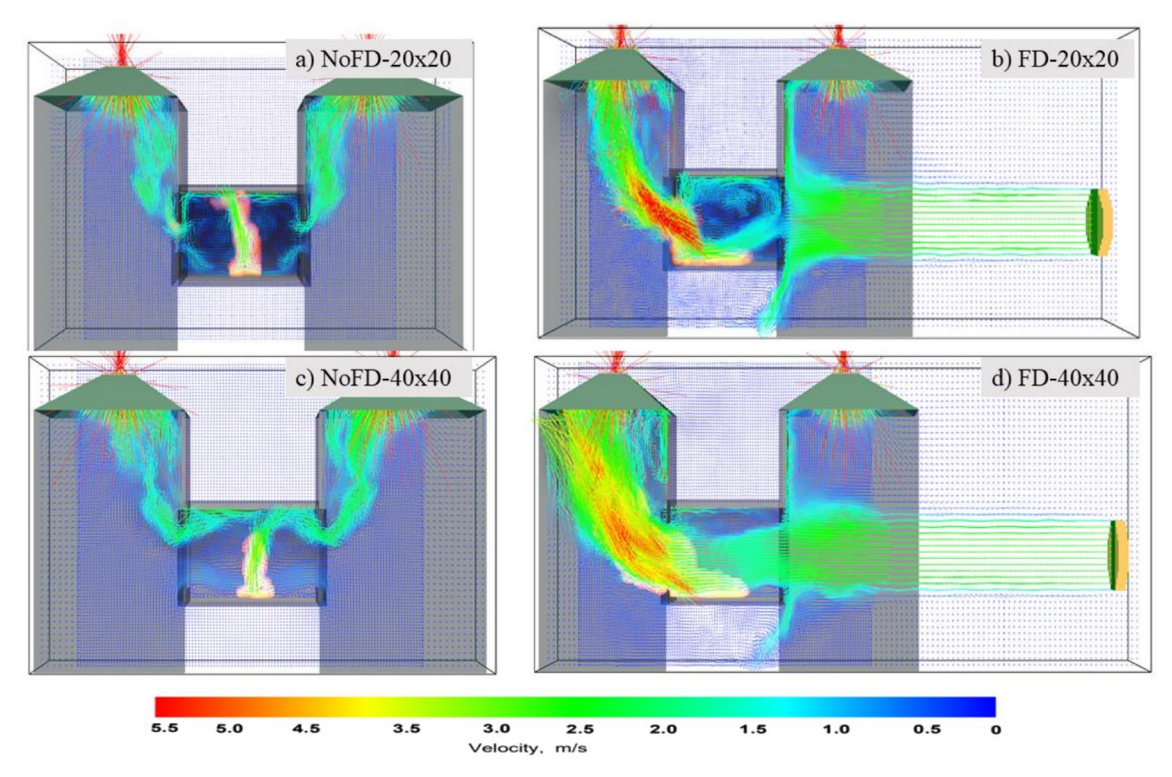


FIGURE 16 | Gas mixture velocity and EVF 150s and 200s after fire initiation under NoFD (a) and (c) and FD (b) and (d) conditions; 20 cm (top) and 40 cm (bottom) opening size.

findings are consistent with previous studies by Hu et al. [25], Ren et al. [44], and Zhao [45], all of which reported reduced flame height and façade temperature with increasing wind velocity.

#### 3.4 | Effect of Wind Velocity on EVF Development

Figure 16a,b depicts predictions of gas mixture velocity and flame locations at 150s after ignition for a 20 cm opening with NoFD and FD conditions (wind speed of 2.9 m/s for FD conditions) respectively. Similarly Figure 16 (c) and (d) depicts predictions of gas mixture velocity and flame location at 200s for 40 cm opening size in both NoFD and FD conditions. Times of 150 and 200s were chosen to ensure that the fire has fully evolved in the compartment, fan was switched on and wind flow was stabilized for both opening sizes.

Under NoFD conditions, as there are two openings in the opposing directions, cold air enters from both sides of the compartment opening resulting in the formation of two recirculation zones inside the compartment (from both sides). For all opening sizes, bidirectional flow is observed as fresh air enters through the bottom part of the opening and hot gases exits through the upper part of the opening. EVF is located closer to the adjacent façade, causing high heat transfer to the facades. As in the case of NoFD, the fire behavior is similar to a conventional compartment fire and air entrainment in the compartment varies primarily with the ventilation factor  $A\sqrt{H}$ , where A represents area of the opening and H represents height of the opening. Higher ventilation factor increases air entrainment rate and higher venting of fire gases exiting from the compartment. Additionally, this can also

influence the gas mixture velocity and flame locations as represented in Figure 16 below.

Under FD conditions, a similar inflow of air from the bottom part of both openings formulates two recirculation zones; however, once the fan induces the presence of wind, the recirculation zones near the openings are no longer visible, and a single recirculation zone in the interior of the fire compartment is created. Only unidirectional flow can be observed for all three opening sizes, where hot gases including flame exit through the entire opening. A similar observation was found in the NoFD condition, as, in all three opening size cases, a bi-directional flow was observed in the experiment.

Additionally, as the area of opening increases, for example, as observed in the case of 40 cm opening size FD-40×40, it is observed that the flame exits through the bottom part and hot gases exit through the upper part of the opening. A maximum velocity of 5.5 m/s was measured for the FD conditions due to the presence of wind speed and EVF flow velocities are relatively low in the NoFD condition for all the cases. The introduction of wind changes the in-compartment fire dynamics, flow behavior, pressure distribution, temperature, velocity and the flame locations. Also, wind creates a positive pressure on the windward side and a negative pressure on the leeward side; further aided by an increase in opening size resulted in a more efficient way of venting hot gases (due to the higher ventilation factor) as EVFs are pushing outwards resulting in higher EVF projection. The results demonstrated that wind significantly impacts the fire dynamics within the compartment. These findings align with a previous study conducted by Beshir [11], which investigated the effect of external wind conditions on fire spread between two informal settlement

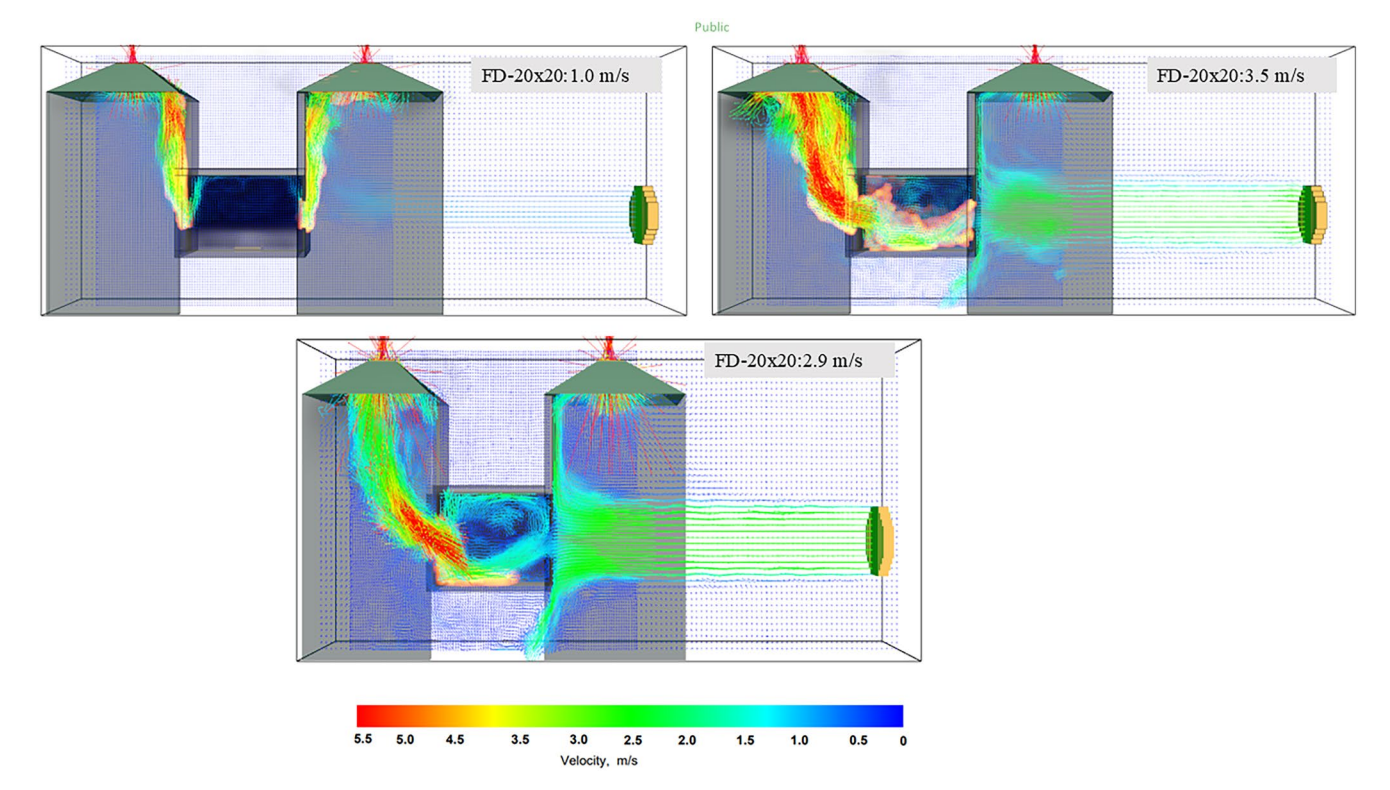
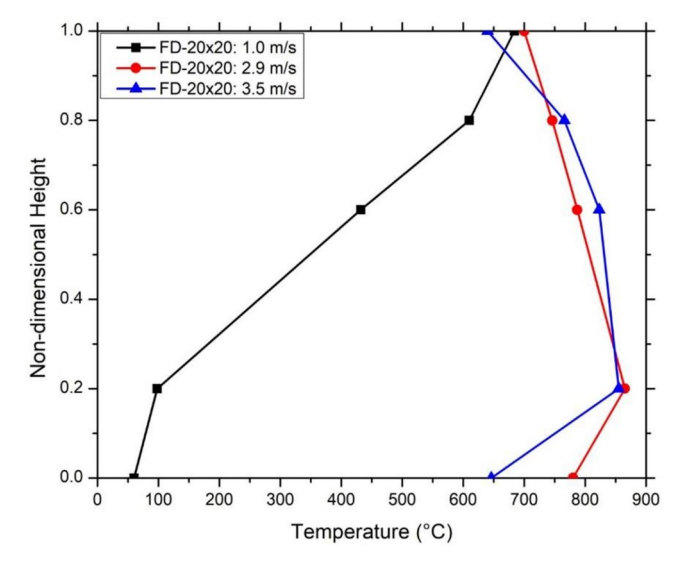


FIGURE 17 | Gas mixture velocity and EVF at 200s after fire initiation under FD condition with different wind velocities.

dwellings spaced 1 m apart. They underscore the critical importance of considering wind effects when assessing the fire safety of buildings, particularly concerning fire separation distances in densely populated areas.

Figure 17 presents the velocity field and EVF characteristics for the FD-20×20 configuration under three different fan inlet velocities: 1.0, 2.9, and 3.5 m/s. The analysis demonstrates the significant influence of wind speed on flame trajectory, façade attachment, and flow symmetry. At 1.0 m/s, the flame behavior closely resembles that of the NoFD condition. Flames emerge symmetrically from both openings with a predominantly vertical projection, maintaining attachment to the façade surfaces. This condition results in increased thermal exposure to the external wall, thereby promoting upward flame spread. As the inlet velocity increases to 2.9 m/s, the incoming airflow causes the flame to tilt toward the leeward opening, resulting in a more pronounced EVF with horizontal projection. At 3.5 m/s, the highest fan velocity condition, the forced draught dominates the flow behavior. The flame is strongly pushed out through a single opening and redirected with a fully tilted profile. EVF under this condition exhibits the longest horizontal projection with intense velocity among the three cases.

To evaluate the thermal impact at the compartment opening under different wind conditions with three velocities. Figure 18 presents the temperature distribution at the opening and the results demonstrate a strong correlation between wind velocity and temperature distribution. At  $1.0\,\mathrm{m/s}$ , the temperatures are significantly lower, particularly at the lower portions of the opening. This is consistent with the observed bi-directional flow. In contrast, at  $2.9\,\mathrm{and}$   $3.5\,\mathrm{m/s}$ , the forced draught conditions dominate the flow field, pushing hot gases and flames directly toward the opening. The



**FIGURE 18** | Non-dimensional vertical distribution of the temperature at the outlet opening with different wind speed.

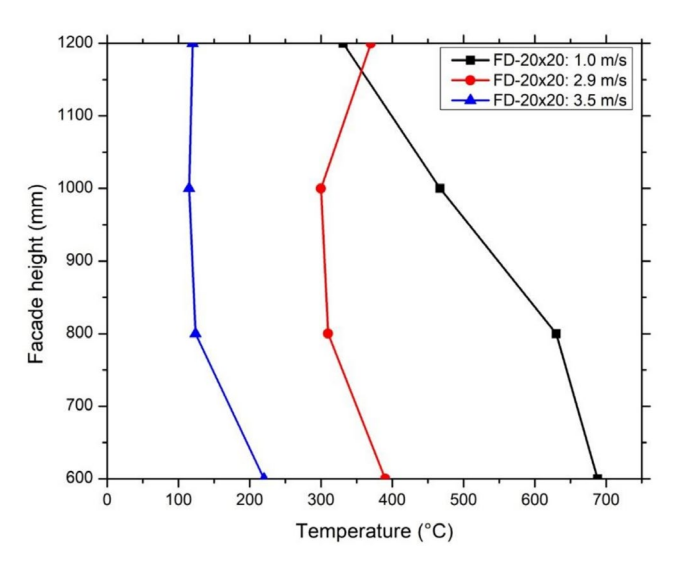
 $3.5\,\mathrm{m/s}$  case shows a slightly broader distribution of high temperatures, indicating a more forceful redirection of the EVF outward.

Figure 19 presents the thermal exposure to the façade. At  $1.0\,\mathrm{m/s}$ , the façade experiences significantly higher temperatures, indicating strong flame attachment to the façade. This condition resembles the NoFD scenario, where the flame rises vertically and remains in contact with the building surface, resulting in higher thermal exposure and potential for upward fire spread. In contrast, for both the 2.9 and  $3.5\,\mathrm{m/s}$  cases, the temperatures at all measured heights are notably lower. This reduction is attributed

to the increased horizontal projection of the externally venting flame (EVF), where the flame is tilted away from the façade due to the imposed wind.

### 3.5 | Oxygen Concentration

Figure 20 depicts the spatial distribution of oxygen concentration inside the compartment at 150s for 20cm opening size (NoFD- $20\times20$  and FD- $20\times20$ ) and 200s for 40cm opening size (NoFD- $40\times40$ ) after fire initiation. A decreased oxygen



**FIGURE 19** | Vertical distribution of the temperature at the facade with different wind speed.

concentration was observed during NoFD conditions compared to FD conditions. As stated previously in temperature field, when fire sustains with consumption of oxygen, oxygen concentration inside the upper part of the compartment decreases and temperature increases. This zone is termed the hot zone, whereas the entrainment of fresh air from the opening resulted in formation a cold zone similar to the temperature field, characterized by lower temperature and higher oxygen concentration.

# 3.6 | Turbulence Model and Forced Draught Impact on EVF

The numerical simulations were conducted using the default turbulence model settings in FDS. However, during the journal submission process, reviewer feedback considered evaluating the influence of different turbulence sub-models to improve the accuracy of the predictions.

Given these findings, it was deemed essential to investigate the influence of different turbulence sub-models on the accuracy of numerical predictions. For this purpose, the FD-40 $\times$ 40 test case was selected for comparative analysis using the turbulence sub-models given in Table 4.

# 3.6.1 │ Temperature at the Opening With Different Turbulence Models

Figure 21 depicts the relationship between non-dimensional height and temperature at the compartment opening with different turbulence models. The data corresponds to five thermocouples placed at discrete vertical positions: 0H, 0.2H, 0.5H,

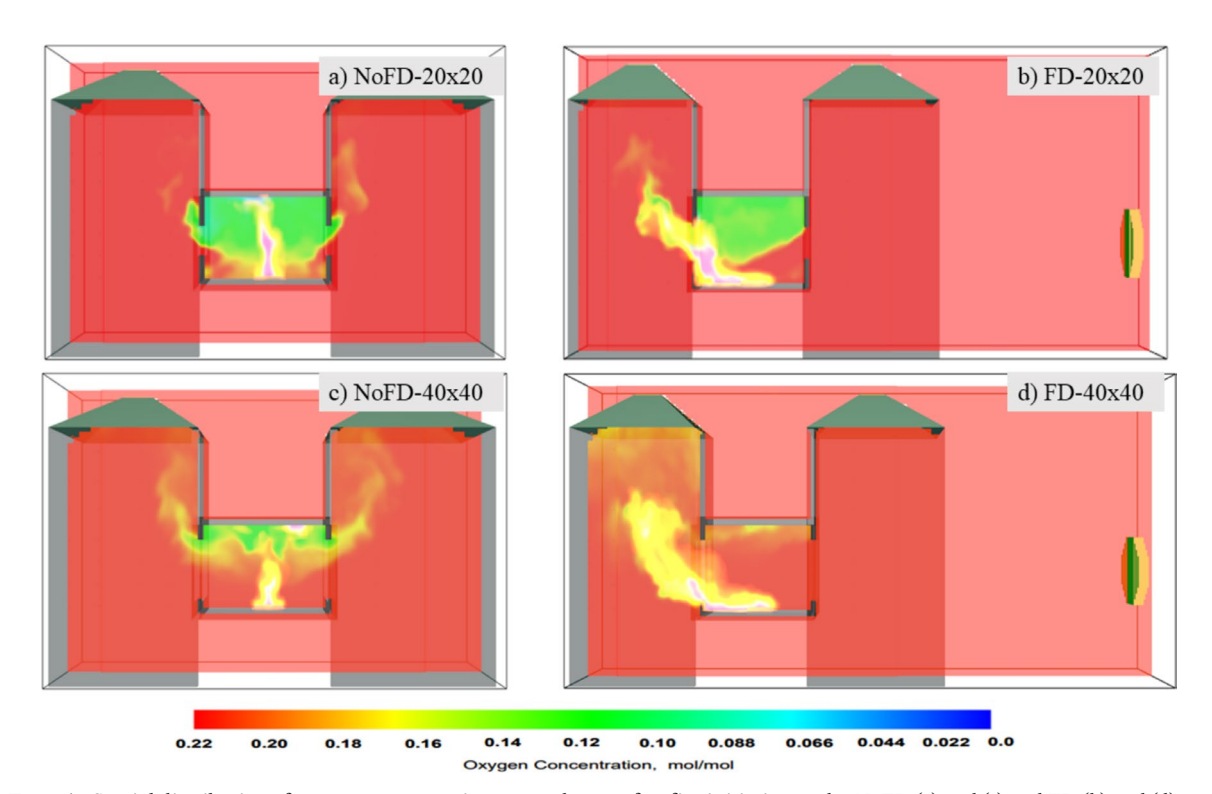


FIGURE 20 | Spatial distribution of oxygen concentration 150 and 200 s after fire initiation under NoFD (a) and (c) and FD (b) and (d) conditions; 20 cm (top) and 40 cm (bottom) opening size.

**TABLE 4** | Turbulence model test scenarios.

Test case	Turbulence sub models
FD-40×40 Deardorff's Model	
	Dynamic Smagorinsky model.
	Vreman's Model.
	Constant Coefficient Smagorinsky model.

**FIGURE 21** | Non-dimensional vertical distribution of the temperature at the outlet opening with turbulence models.

Temperature (°C)

0.75H, and H, where H represents the full height of the opening (40 cm) in the FD 40  $\times$  40 experimental configuration. The thermocouple layout is shown in Figure 4 for reference. Consistent with the methodology presented in Section 3.1, the temperature values represent a 20-s time-averaged period during peak fire conditions for all turbulence model cases under consideration.

Figure 21 illustrates the non-dimensional height versus temperature profile for the FD-40×40 test case, comparing experimental data with FDS simulations using four different turbulence sub-models: Deardorff, Vreman, Constant Smagorinsky, and Dynamic Smagorinsky. The non-dimensional height represents five thermocouple locations distributed along the opening height (H=0.4m). The FDS default model (Deardorff) showed significant deviations from the experimental temperature profile, particularly at the bottom and mid height levels with an error margin exceeding 40%. Both the Vreman and Constant Smagorinsky models also demonstrated noticeable overpredictions, especially at higher elevations. In contrast, the Dynamic Smagorinsky model yielded temperature predictions that closely followed the experimental trend across most of the thermocouple heights. Although it exhibited a slight overestimation, the temperature deviation remained within a 10% margin, indicating a good level of agreement with experimental result and in capturing the outward flow and stratification dynamics within the compartment and at the compartment opening. This comparison highlights the critical influence of turbulence model selection on compartment fire scenario under forced draught conditions with large openings.

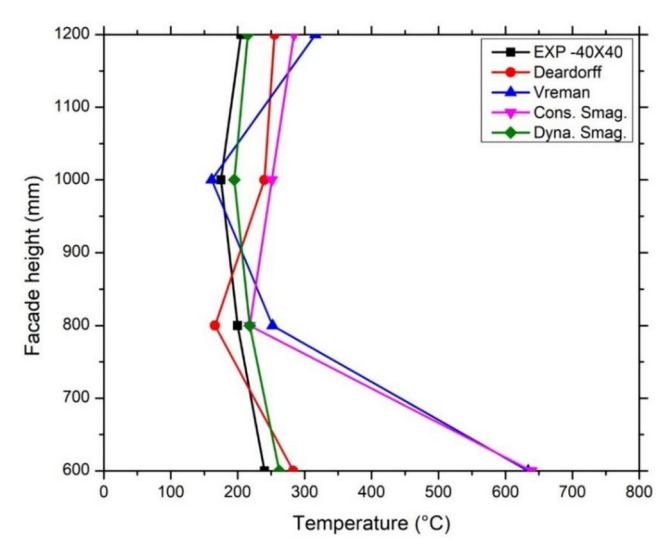


**FIGURE 22** | Vertical distribution of the temperature at the centerline of the outlet façade with different turbulence models.

# 3.6.2 │ Temperature at the Façade With Different Turbulence Model

Thermocouples were positioned in the façade as depicted in the Figure 3. Figure 22 presents the facade temperature distribution along vertical heights ranging from 600 to 1200 mm for the FD- $40\times40$  test case.

The comparison includes experimental measurements and simulation results obtained from FDS using four different turbulence sub-models. Among the simulation models, the Deardorff and Dynamic Smagorinsky sub-models show reasonable alignment with the experimental trend. The constant Smagorinsky and Vreman Models, however, tend to significantly overpredict temperatures, with the Vreman Model showing values exceeding 600°C—more than double the experimental peak. Overall, the dynamic Smagorinsky Model maintain the good alignment with the experimental results and shows the best physical representation and maintaining error margins in less than 10% of the experimental values.

### 4 | Conclusions

The present study focuses on the impact of ventilation conditions on the development of EVF and its impact on the façade in medium-scale configurations. A numerical model was used and validated with the experimental results to investigate what the effect of different wind velocities and opening sizes is on the EVF development and its impact on the façade of the outlet opening.

The effect of opening size on the EVF thermal characteristic and on the façade was experimentally and numerically investigated. As experimentally investigated, under FD conditions, the thermal impact on the façade wall is reduced compared to NoFD conditions as the wind pushes EVF in the outward direction from the outlet opening and thus increases EVF projection. This is an important aspect to consider when determining the fire separation distance between buildings for the fire and

life safety design of structures. Notably, in NoFD conditions, an average temperature increase exceeding 30% was observed for the 20cm case, while the temperature increased by 150% and 200% for the 30 and 40 cm NoFD cases, respectively. Also, the overall projection of the EVF for FD conditions is higher compared to NoFD as indicated by the maximum recorded experimental measurements. The maximum temperature observed at the top of the window lintel is 870°C for the FD 20×20 case and 430°C for the NoFD case. This is another critical aspect to consider when selecting façade materials, designing horizontal fire barriers, and implementing passive fire stopping measures in building design. Numerical results of NoFD conditions are in good agreement with experimental results as there is a 6% variance but this was increased to 15% when compared with experimental measurements of temperature under FD conditions. As indicated in both experimental and numerical work, results are in good agreement, and the numerical model is able to predict the phenomena of compartment fire development both inside and outside the compartment. This numerical model can be used with confidence as part of the performance-based design in building fire and life safety design.

It was revealed that opening size has significant influence on the development and temperature distribution of EVF under both NoFD and FD conditions, as increased opening resulted in different flow fields and reoutlining recirculation zones near the openings. For increased opening sizes, the vertical distribution of the temperature profile at the centerline of the outlet at the façade yielded increased gas temperatures. Under FD conditions, for all different sizes, the façade temperatures recorded were decreased compared to NoFD conditions. Numerical results of facade temperatures under NoFD conditions for 20 and 40 cm cases, are in good agreement with experimental results as there is 7% variance. This increased to 10% when compared with experimental measurements of temperature under FD conditions. Stratification of the gas layer at the interior of the fire compartment was not observed during FD conditions as there was increased mixing of air due to the presence of wind, as also observed from the analysis of the gas mixture velocity profile for different opening sizes where a maximum of 5.5 m/s was calculated for the FD-40×40 case. This is supported by the decreased oxygen concentration observed during NoFD conditions compared to FD conditions due to the introduction of wind and this changes the in-compartment fire dynamics, flow behavior, temperature, velocity, and the flame locations.

Numerical modelling has predicted the temperature profile reasonably well when smaller compartment opening sizes are considered. However, when the opening size is increased, and the wind factor is introduced the model becomes more complex and the relevant error difference was in the range of 30% or more. As the default Deardorff model in FDS, and the results were not in good agreement with the experimental result, and this prompted further investigation into alternative turbulence models to improve simulation accuracy. The results indicate that while all models capture the general EVF trends, the Dynamic Smagorinsky model provided the closest agreement with experimental data in terms of temperature distribution and EVF shape, with less than 10% error. In contrast, other models like Vreman and Constant Smagorinsky significantly overpredicted temperature profiles, especially at the façade and opening

regions. This study also highlights the importance of turbulence model selection, particularly in scenarios involving complex wind and opening interactions, and supports the use of dynamic models for improved predictive accuracy in future fire safety simulations.

Overall, this study highlights the critical importance of considering ventilation conditions in fire safety design and the necessity of precise modeling to predict fire behavior and its impact on building structures. The insights gained from this research can shape fire safety regulations and lead to the development of more effective fire protection strategies, ultimately enhancing the safety and resilience of building designs.

#### Acknowledgments

The project was financially funded by NGO Majaczech, z.s. (Czech Fire Protection Association). Additionally, the authors wish to thank the Central Firefighting School in Bile Policany for providing space and equipment for this work.

#### **Conflicts of Interest**

The authors declare no conflicts of interest.

#### **Data Availability Statement**

The data that support the findings of this study are available from the corresponding author upon reasonable request.

#### References

- 1. D. Drysdale, An Introduction to Fire Dynamics, 3rd ed. (John Wiley & Sons, 2011).
- 2. J. G. Quintiere, Principles of Fire Behavior, 2nd ed. (CRC Press, 2016).
- 3. E. Asimakopoulou, D. Kolaitis, and M. Founti, "Performance of a Ventilated-façade System Under Fire Conditions: An Experimental Investigation," *Fire and Materials* 44, no. 6 (2020): 776–792, https://doi.org/10.1002/fam.2863.
- 4. M. Bonner, W. Wegrzynski, B. Papis, and R. G. Kresnik, "A Top-Down, Statistical Approach to Understand the Fire Performance of Building Facades Using Standard Test Data," *Building and Environment* 169 (2020): 106540, https://doi.org/10.1016/j.buildenv.2019.106540.
- 5. E. K. Asimakopoulou, K. Chotzoglou, D. I. Kolaitis, and M. A. Founti, "Characteristics of Externally Venting Flames and Their Effect on the Façade: A Detailed Experimental Study," *Fire Technology* 52 (2016): 2043–2069, https://doi.org/10.1007/s10694-016-0575-5.
- 6. J. Smolka, K. Kempna, P. Danihelka, et al., "Wind Driven (Forced Draught) Impact on Enclosure Fires," in *Applications of Structural Fire Engineering* (University of Ljubljana, 2021).
- 7. D. Madrzykowski and S. Kerber, Fire Fighting Tactics Under Wind-Driven Conditions: Laboratory Experiments. Technical Note (National Institute of Standards and Technology, 2009).
- 8. M. Li, Z. Gao, J. Ji, K. Li, and J. Sun, "Wind Effects on Flame Projection Probability From a Compartment With Opposing Openings," *Fire Safety Journal* 91 (2017): 414–421, https://doi.org/10.1016/j.firesaf.2017.04.037.
- 9. H. Huang, R. Ooka, N. Liu, L. Zhang, Z. Deng, and S. Kato, "Experimental Study of Fire Growth in a Reduced-Scale Compartment Under Different Approaching External Wind Conditions," *Fire Safety Journal* 44, no. 3 (2009): 311–321, https://doi.org/10.1016/j.firesaf. 2008.07.005.

- 10. J. Ji, M. Li, K. Li, M. Yuan, and J. Sun, "Ambient Wind Effect on Combustion Characteristics in a Compartment With Both Door and Window Open," *Energy and Buildings* 105 (2015): 217–225, https://doi.org/10.1016/j.enbuild.2015.07.046.
- 11. M. Beshir, M. Mohamed, S. A. Kouritem, C. K. Lemmertz, F. R. Centeno, and D. Rush, "Investigating Numerically the Effect of Wind on Fire Spread Between Two Informal Settlement Dwellings," *Fire Technology* 61, no. 3 (2023): 1233–1268, https://doi.org/10.1007/s10694-023-01374-y.
- 12. BBC, Dubai's Torch Tower Catches Fire for Second Time in Two Years. BBC News Middle East. Accessed June 21, 2022 (2017), https://www.bbc.com/news/world-middle-east-40822269.
- 13. BBC, Dubai Hotel Fire: The Address Downtown Hotel Engulfed in Flames. BBC News Middle East. Accessed June 21, 2022 (2015), https://www.bbc.com/news/av/world-middle-east-35208484.
- 14. J. Hanna, A. Fantz, and C. E. Shoichet, Fire Engulfs Downtown Dubai's High-Rise Address Hotel. CNN. Accessed June 21, 2022 (2015), https://edition.cnn.com/2015/12/31/middleeast/dubai-address-hotel-fire/index.html.
- 15. A. Dodd, "The Cladding Conundrum: Discussing the Valencia High-Rise Fire," *International Fire & Safety Journal* 3, no. 34 (2024): 106–108.
- 16. S. Hansen, "Evaluation of Fire Spread in the Large Lærdal Fire," in *Proceedings of the 14th International Fire and Materials Conference and Exhibition* (2015), 1014–1024.
- 17. J. Fahd, Fire Investigation Report of Findings. Cohoe: Homeland Security and Emergency Services. Accessed June 22, 2022 (2017), https://www.edgewood.edu/docs/default-source/aboutdocs/2018-security-and-fire-safety-report.pdf.
- 18. E. K. Asimakopoulou, D. I. Kolaitis, and M. A. Founti, "Assessment of Fire Engineering Design Correlations Used to Describe the Geometry and Thermal Characteristics of Externally Venting Flames," *Fire Technology* 53, no. 2 (2017): 709–739, https://doi.org/10.1007/s10694-016-0594-2.
- 19. EN 1991-1-2, Eurocode 1: Actions on Structures, Part 1-2—General Actions—Actions on Structures Exposed to Fire (European Committee for Standardization, 2002).
- 20. Y. Abu-Zidan, S. Rathnayaka, P. Mendis, and K. Nguyen, "Effect of Wind Speed and Direction on façade Fire Spread in an Isolated Rectangular Building," *Fire Safety Journal* 129 (2022): 103570, https://doi.org/10.1016/j.firesaf.2022.103570.
- 21. L. Hu, J. A. Milke, and B. Merci, "Special Issue on Fire Safety of High-Rise Buildings," *Fire Technology* 53, no. 1 (2017): 1–3, https://doi.org/10.1007/s10694-016-0638-7.
- 22. Y. P. Lee, M. A. Delichatsios, and G. W. H. Silcock, "Heat Fluxes and Flame Heights in façades From Fires in Enclosures of Varying Geometry," *Proceedings. Combustible Institute* 31, no. 2 (2007): 2521–2528, https://doi.org/10.1016/j.proci.2006.08.033.
- 23. X. Sun, F. Tang, K. Lu, et al., "Fundamentals of Window-Ejected Fire Plumes From Under-Ventilated Compartment Fires: Recent Progress and Perspectives," *Progress in Energy and Combustion Science* 94 (2023): 101039, https://doi.org/10.1016/j.pecs.2022.101039.
- 24. J. M. Li, C. C. Yin, C. Hu, Y. F. Li, and P. Xu, "Computational Study of Wind Effect on Window Flame Spread Across the Exterior Wall of High-Rise Buildings," *Applied Mechanics and Materials* 438–439 (2013): 1898–1902.
- 25. L. Hu, K. Hu, F. Ren, and X. Sun, "Facade Flame Height Ejected From an Opening of a Fire Compartment Under External Wind," *Fire Safety Journal* 92 (2017): 151–158, https://doi.org/10.1016/j.firesaf.2017. 06.008.
- 26. M. Li, Z. Gao, J. Ji, and H. Wan, "External Wind Effect on Flame Behavior Inside and Outside a Compartment With Opposing Openings," *Fire Technology* 57 (2021): 1987–2006, https://doi.org/10.1007/s10694-021-01104-2.

- 27. W. Gao, N. Liu, M. Delichatsios, et al., "Fire Spill Plume From a Compartment With Dual Symmetric Openings Under Crosswind," *Combustion and Flame* 167 (2016): 409–421, https://doi.org/10.1016/j.combustflame.2016.01.011.
- 28. H. X. Chen, N. A. Liu, and W. K. Chow, "Wind Tunnel Tests on Compartment Fires With Crossflow Ventilation," *Journal of Wind Engineering and Industrial Aerodynamics* 99, no. 10 (2011): 1025–1035, https://doi.org/10.1016/j.jweia.2011.07.006.
- 29. A. Lönnermark and H. Ingason, The Effect of Cross-Sectional Area and Air Velocity on the Conditions in a Tunnel During a Fire. SP Report. SP Technical Research Institute of Sweden. Accessed June 21, 2022 (2007), https://www.diva-portal.org/smash/get/diva2:962400/FULLTEXT01.pdf.
- 30. S. McAllister and M. Finney, "The Effect of Wind on the Burning Rate of Wood Cribs," *Fire Technology* 52 (2016): 1035–1050, https://doi.org/10.1007/s10694-015-0536-4.
- 31. K. Himoto, T. Tsuchihashi, Y. Tanaka, and T. Tanaka, "Modeling Thermal Behaviors of Window Flames Ejected From a Fire Compartment," *Fire Safety Journal* 44, no. 2 (2009): 230–240, https://doi.org/10.1016/j.firesaf.2008.06.005.
- 32. L. Hu, X. Sun, X. Zhang, and F. Ren, "Facade Flame Height and Horizontal Extending Distance From the Opening of a Compartment Fire With External Sideward Wind," *Proceedings of the Combustion Institute* 37, no. 3 (2019): 3859–3867, https://doi.org/10.1016/j.proci.2018.06.201.
- 33. J. Smolka, The Effect of Forced Draught on the Externally Venting Flame Parameters of Enclosure Fire. PhD Thesis, Technical University of Ostrava, Czech Republic (2022).
- 34. J. G. Quintiere, Fundamentals of Fire Phenomena (John Wiley & Sons Ltd, 2006).
- 35. J. Smolka, Scale Base for Load Cell by Majaczech. Thingiverse. Accessed July 26, 2022 (2020), https://www.thingiverse.com/thing: 4330707.
- 36. OMEGA, Wire Colour Codes and Limits of Error. Omega Engineering Inc. Accessed April 3, 2023 (2023), https://in.omega.com/techref/colorcodes.html.
- 37. J. Smolka, K. Kempná, P. Kučera, K. Kempný, E. Asimakopoulou, and P. Danihelka, "Setup of a 3D Printed Wind Tunnel: Application for Calibrating Bi-Directional Velocity Probes Used in Fire Engineering Applications," *HardwareX* 15 (2023): e00440, https://doi.org/10.1016/j.ohx.2023.e00440.
- 38. B. J. McCaffrey and G. Heskestad, "A Robust Bidirectional Low-Velocity Probe for Flame and Fire Application," *Combustion and Flame* 26, no. 1 (1976): 125–127, https://doi.org/10.1016/0010-2180(76)90062-6.
- 39. K. McGrattan, S. Hostikka, R. McDermott, J. Floyd, C. Weinschenk, and K. Overholt, Fire Dynamics Simulator User's Guide. NIST Special Publication 1019 (2019).
- 40. A. Hamins, A. Maranghides, and G. W. Mulholland, The Global Combustion Behavior of 1 MW to 3 MW Hydrocarbon Spray Fires Burning in an Open Environment. US Department of Commerce, National Institute of Standards and Technology. Accessed July 26, 2022 (2003).
- 41. W. Węgrzyński, T. Lipecki, and G. Krajewski, "Wind and Fire Coupled Modeling—Part II: Good Practice Guidelines," *Fire Technology* 54, no. 5 (2018): 1443–1485, https://doi.org/10.1007/s10694-018-0749-4.
- 42. J. Smagorinsky, "General circulation experiments with the primitive equations: I. The basic experiment," *Monthly Weather Review* 91, no. 3 (1963): 99–164, https://doi.org/10.1175/1520-0493(1963)091<0099: GCEWTP>2.3.CO;2.
- 43. T. Okaze, H. Kikumoto, H. Ono, et al., "Benchmark Test of Flow Field Around a 1:1:2 Shaped Building Model Using LES: Influences of Various Calculation Conditions on Simulation Results," *AIJ Journal of Technology and Design* 26, no. 62 (2020): 179–184, https://doi.org/10.3130/aijt.26.179.

44. F. Ren, L. Hu, X. Sun, and K. Hu, "An Experimental Study on the Vertical Temperature Profile of Façade Fire Plume Ejected From a Compartment With an Opening Subjected to External Wind Normal to the Façade," *International Journal of Thermal Sciences* 130 (2018): 94–99, https://doi.org/10.1016/j.ijthermalsci.2018.04.008.

45. Z. Guoxiang, Numerical Study on Under-Ventilated Enclosure Fires and Fire Spread on Building Façades. PhD Thesis (University of Gent, Belgium, 2017).